




## The Role of Faults as Barriers in Confined Seismic Sequences: 2021 Seismicity in the Granada Basin (Betic Cordillera)

Asier Madarieta-Txurruka<sup>1</sup> , Lourdes González-Castillo<sup>1</sup>, José A. Peláez<sup>2</sup> , Manuel Catalán<sup>3</sup>, Jesús Henares<sup>4</sup>, Antonio J. Gil<sup>5,6</sup> , Francisco Lamas-Fernández<sup>7</sup>, and Jesús Galindo-Zaldívar<sup>1,8</sup>

<sup>1</sup>Departamento de Geodinámica, Universidad de Granada, Granada, Spain, <sup>2</sup>Departamento de Física, Universidad de Jaén, Jaén, Spain, <sup>3</sup>Real Instituto y Observatorio de la Armada, San Fernando, Spain, <sup>4</sup>Universidad Internacional de La Rioja, Logroño, La Rioja, Spain, <sup>5</sup>Departamento Ing. Cartográfica, Geodésica y Fotogrametría, Universidad de Jaén, Jaén, Spain, <sup>6</sup>Centro de Estudios Avanzados en Ciencias de la Tierra, Energía y Medio Ambiente (CEACTEMA), Universidad de Jaén, Jaén, Spain, <sup>7</sup>Departamento de Ingeniería Civil, Universidad de Granada, Granada, Spain, <sup>8</sup>Instituto Andaluz de Ciencias de la Tierra (CSIC-UGR), Granada, Spain

### Key Points:

- The Granada 2021 seismicity is related to the activity of a 2 km NW-SE normal fault segment bounded by oblique faults acting as barriers
- The confined seismic activity extended vertically due to preexisting intense brittle deformation of the basement
- The seismic barriers responsible for a swarm evolving to mainshock-aftershock behavior decreased the seismic potential by some extent

### Correspondence to:

A. Madarieta-Txurruka,  
amadatu@ugr.es

### Citation:

Madarieta-Txurruka, A., González-Castillo, L., Peláez, J. A., Catalán, M., Henares, J., Gil, A. J., et al. (2022). The role of faults as barriers in confined seismic sequences: 2021 seismicity in the Granada Basin (Betic Cordillera). *Tectonics*, *41*, e2022TC007481. <https://doi.org/10.1029/2022TC007481>

Received 27 JUN 2022

Accepted 8 SEP 2022

### Author Contributions:

**Conceptualization:** Asier Madarieta-Txurruka, Lourdes González-Castillo, Jesús Galindo-Zaldívar

**Data curation:** José A. Peláez, Manuel Catalán, Jesús Henares, Antonio J. Gil, Francisco Lamas-Fernández

**Formal analysis:** Asier Madarieta-Txurruka, José A. Peláez, Manuel Catalán, Jesús Henares, Antonio J. Gil

**Funding acquisition:** José A. Peláez, Antonio J. Gil, Jesús Galindo-Zaldívar

**Investigation:** Asier Madarieta-Txurruka, Lourdes González-Castillo, José A. Peláez, Jesús Galindo-Zaldívar

© 2022. The Authors.

This is an open access article under the terms of the [Creative Commons Attribution-NonCommercial-NoDerivs License](https://creativecommons.org/licenses/by/4.0/), which permits use and distribution in any medium, provided the original work is properly cited, the use is non-commercial and no modifications or adaptations are made.

**Abstract** Fault barriers are key structures for studying seismic hazard in regions of intense brittle deformation. The interaction between fault sets affects their seismogenic behavior, if some of them act as barriers. The Granada Basin, in the Betic Cordillera, is a region affected by shallow brittle deformation, as it was the scenario for the recent Granada 2021 seismic sequence. This seismicity presented a swarm behavior at the beginning of the sequence, followed by mainshock-aftershock features. Geological and gravity data presented here reveal that the basement is affected by two sets of NW-SE and NE-SW normal faults and intensely deformed by vertical NW-SE joints. Improved relocation of the Granada 2021 seismicity reveals a confined chimney-shape seismicity caused by the activity of a 2 km long NW-SE normal fault segment. The confinement of the sequence is associated with the NE-SW fault set acting as a barrier that restricts the rupture area, limiting the maximum magnitude, and favoring the recurrence of events with smaller magnitude. The chimney-shape of the seismic sequence suggests that the deformation is propagated vertically to the surface, facilitated by preexisting fractures. The shallow extensional deformation during the uplift of the central Betic Cordillera drove the activity of the local structures obliquely to the regional extensional trends, as evidenced by the seismic sequence. This multidisciplinary study improves the knowledge on the origin of the Granada Basin and underlies the important role of preexisting fractures on fault segmentation and seismic propagation, decreasing the seismic potential of this area.

## 1. Introduction

The seismic sequence behavior is featured in between two end-members: mainshock-aftershock sequences and swarms. The mainshock-aftershock sequences characterize by a main event that usually occurs at the beginning of the sequence—sometimes preceded by foreshocks—due to tectonic stress accumulation on the main fault. Usually, the aftershocks are directly triggered by the main earthquake (e.g., Vidale & Shearer, 2006), or another aftershock (Ogata, 1988). They delineate the rupture surface (Scholz, 1990) and usually propagate along the main fault toward other segments (Henry & Das, 2001). Therefore, the aftershocks are attributed to a cascade of elastic fault rupture following Omori's law (Omori, 1895). In addition, aftershocks can also occur due to dynamic triggering (Freed, 2005; Gomberg & Johnson, 2005; Hill & Prejean, 2015; among others) or postseismic stress transfer and strength weakening (e.g., Cattania et al., 2015; Freed, 2005).

However, the swarms do not have an earthquake of sufficient magnitude to explain the extension of the epicentral distribution and the extended duration (Mogi, 1963), and the largest earthquake does not usually start the sequence. Swarms are often related to volcanic phenomena (Benoit & McNutt, 1996; Endo et al., 1981; Hill, 1977; Hurst & McGinty, 1999; McNutt, 1996; Power et al., 1994; among others) and geothermal regions (Dziak et al., 2003; Hainzl & Fischer, 2002). However, they can also occur in tectonically active contexts, whether on plate boundaries (e.g., Hamdache et al., 2019, 2016; Llenos et al., 2009; Lohman & McGuire, 2007; Vidale et al., 2006; Vidale & Shearer, 2006) or interplate rifts (e.g., Ibs-von Seht et al., 2008; Stankova et al., 2008). This type of seismic sequence is often attributed to areas of the crust with many heterogeneities (Udías & Mezcuca, 1986), to hidden influence of fluids (Hatch et al., 2020; Špičák et al., 2005), or to near aseismic fault-slip (Hatch et al., 2020;

**Methodology:** Asier Madarieta-Txurruka, Antonio J. Gil, Jesús Galindo-Zaldívar

**Project Administration:** Jesús

Galindo-Zaldívar

**Resources:** José A. Peláez, Antonio J.

Gil, Jesús Galindo-Zaldívar

**Software:** José A. Peláez, Antonio J. Gil,

Jesús Galindo-Zaldívar

**Supervision:** Lourdes González-Castillo,

Jesús Galindo-Zaldívar

**Validation:** Lourdes González-Castillo,

Jesús Galindo-Zaldívar

**Visualization:** Asier Madarieta-Txurruka,

Manuel Catalán

**Writing – original draft:** Asier

Madarieta-Txurruka

**Writing – review & editing:** Lourdes

González-Castillo, José A. Peláez,

Manuel Catalán, Jesús Henares, Antonio

J. Gil, Francisco Lamas-Fernández, Jesús

Galindo-Zaldívar

McGuire et al., 2005; Roland & McGuire, 2009), and are often characterized by a hypocenter migration (e.g., Hainzl, 2004; Hayashi & Morita, 2003; Kyriakopoulos et al., 2013; Waite & Smith, 2002).

The features of earthquake sequences are influenced by previous brittle heterogeneities (Mogi, 1963; Udías & Mezcuca, 1986). Although pre-existing fractures act as zones of weakness that facilitate rupture propagation, they could also act as fault barriers if their orientation with respect to stress is not compatible to be reactivated. Barriers are key to constrain the boundaries between zones with different coupling (Chlieh et al., 2008), to delimit the rupture area (RA) during a single earthquake (Aki, 1979), and finally, to estimate the expected magnitude of the seismogenic fault (e.g., Leonard, 2010; Wells & Coppersmith, 1994). There are many controlling factors that affect the barriers in parallel normal fault segments (Harris, 1998, 2004), including the mechanical interaction and stress triggering from nearby structures. Consequently, intersections between seismogenic faults and perpendicular or oblique faults can act as barriers as long as they segment and misalign the seismogenic ones. What role do intersections between faults play in segmentation and barrier formation? How do barriers affect the sequence evolution and deformation migration? To answer these questions, it is important to keep in mind that a mechanical interaction between faults or segments does not imply a synchronous rupture, but that faults are not independent (DuRoss & Hylland, 2015). Mechanically interacting faults would be those that determine the displacement and stress and earthquake distribution of nearby faults (Gupta & Scholz, 2000; Peacock & Sanderson, 1991; Scholz & Gupta, 2000; Willemse et al., 1996).

The Granada Basin, located in the central Betic Cordillera (Figure 1), is characterized by the intersection of orthogonal or oblique normal faults and related high brittle deformation of the crust, derived from the Neogene-Quaternary evolution of the Betic Cordillera. Located in the central Betic Cordillera (Southern Iberia), it is an extensional basin developed since the middle Miocene (Braga et al., 1990) due to the activity of normal faults (Morales et al., 1990; Rodríguez-Fernández & Sanz de Galdeano, 2006). Currently, it presents a shallow seismic activity of low to low-moderate magnitudes (Galindo-Zaldívar et al., 1999; Morales et al., 1997). Seismicity is related to the activity of high- and low-angle normal faults (Madarieta-Txurruka et al., 2021; Rodríguez-Fernández et al., 2012). Seismic sequences have been documented throughout recent history, the last one occurring during the year 2021. This sequence was felt in the metropolitan area of the city of Granada, reaching up to an  $m_{bLg}$  4.6 earthquake (Informe IGN, 2021). There are different sets of high-angle normal faults and joints that interact with each other, the most important of which are NW-SE and NE-SW fault sets. The activity of the NW-SE faults is known (Sanz de Galdeano et al., 2012, 2003), however, the role played by the NE-SW fault set had not yet been studied in detail. Not only for their possible activity but also for the role they play in the segmentation and formation of barriers. Therefore, the characterization of the interaction between the different fault sets is key to understand the causes and evolution of the 2021 seismic sequence.

Understanding the occurrence of seismic sequence in relation to zones of extended brittle deformation and segmentation of faults, such as the Granada Basin (Figure 1b), requires a multidisciplinary approach. Combined geological and geophysical studies are crucial to shed light on the structures that cause the seismicity. An accurate location of seismicity and earthquake focal mechanism inversion is necessary to localize the rupture and determine the kinematic behavior. At the same time, it is necessary to adequately characterize the structural, kinematic, and recent activity of outcropping faults. In this way, surface structures can be correlated with the active segments in depth (Keller & Pinter, 1996). However, not all seismicity can be explained by outcropping structures. Therefore, it is important to use techniques that make it possible to determine structures in depth. The basement morphology of young sedimentary basins can give us clues in this respect, and it can be studied by gravity analysis due to the density contrast of the sedimentary infill and the basement (Morales et al., 1990; Telford et al., 1990). Finally, geodesy by means of continuous GPS (CGPS) data is the most accurate technique for quantifying surface deformation (Dixon, 1991; Garate et al., 2015; Hager et al., 1991; Koulali et al., 2011; Sagiya et al., 2000; Sparacino et al., 2020). The comparison of geodetic deformation trends with the reduced stress tensor of the seismic sequence will allow us to frame the seismicity in the recent evolution of the central Betic Cordillera.

This research aims to analyze the origin and features of the Granada 2021 seismic sequence by improving the location of the seismicity, determining in detail the structure of the affected zone and establishing the local stress regime, as well as the regional deformation. In this way, it will be possible to better understand the role of the preexisting brittle deformations and the interaction of different sets of faults in the characteristics that highlight the development and evolution of this type of seismic sequence. At the same time, it will allow framing of the



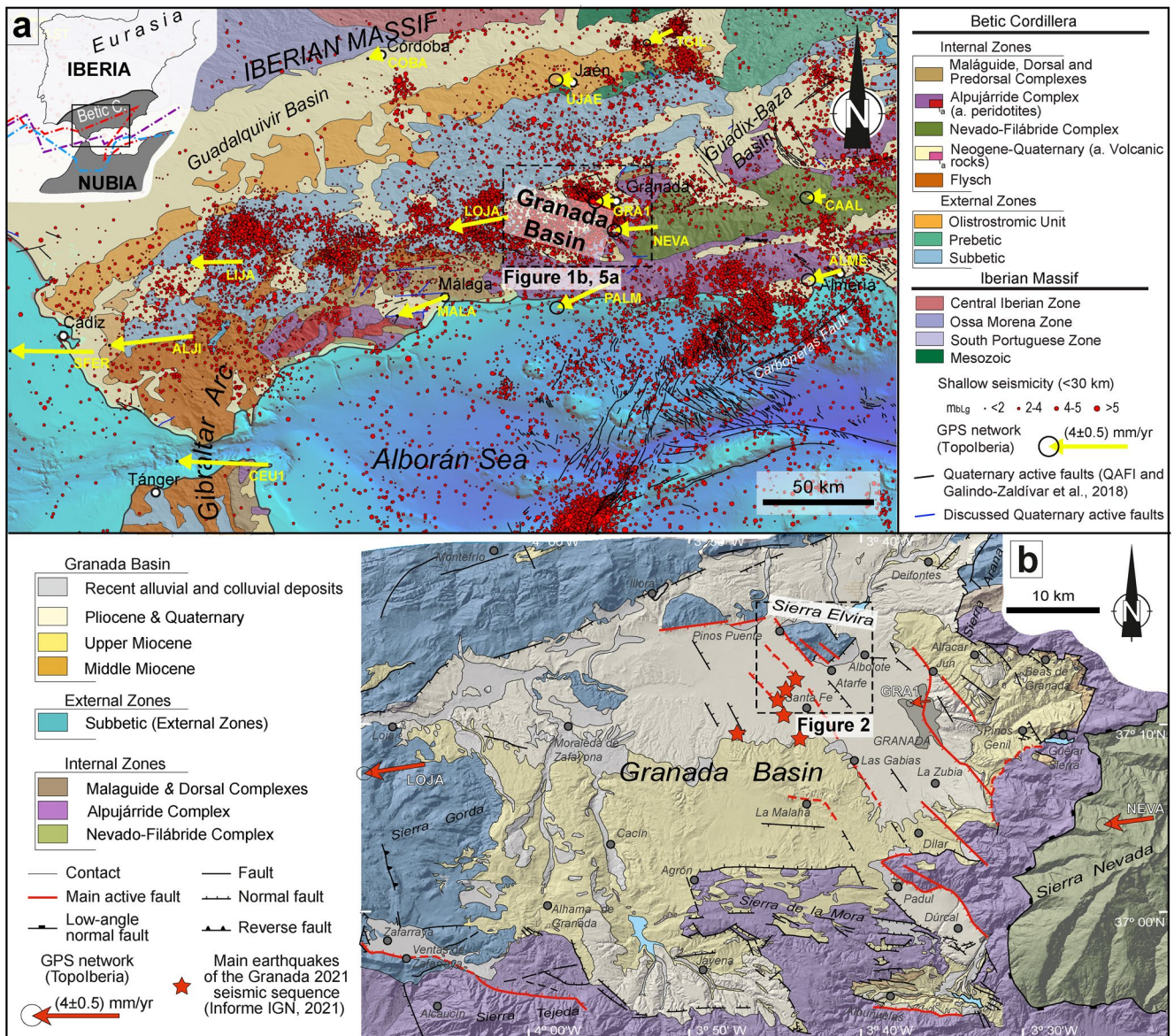


**Figure 1.** Geological and seismological setting of the Granada Basin. (a) Geological map and active quaternary faults (Galindo-Zaldívar et al., 2018; QAFI, 2022) of the western Betic Cordillera. The seismicity since 1900 and < 30 km depth is depicted (SIS, 2022). Yellow arrows represent CGPS data (Galindo-Zaldívar et al., 2015; González-Castillo et al., 2015). Insets: different hypotheses of Iberia-Nubia plate boundary in purple (Klitgord & Schouten, 1986), light blue (Bird, 2003), and red (Gutscher, 2004). (b) Geologic map of the Granada Basin and the main active faults of the Granada Basin faults system (Madarieta-Txurruka et al., 2021; Sanz de Galdeano et al., 2003). Modified from Galindo-Zaldívar et al. (2015). The main earthquakes of the Granada 2021 seismic sequence located by the Spanish Instituto Geográfico Nacional (IGN) are depicted as red stars.

seismicity in the recent evolution of the Betic Cordillera. Finally, the determination of seismogenic fault segments will improve the study of the seismic hazard in an area with high population-density.

## 2. Geological and Seismological Setting

The seismic sequence of January 2021 occurred in the Granada Basin, central Betic Cordillera (Figure 1), and is framed in the context of the collision between the Eurasian and Nubian plates in its westernmost sector of the Mediterranean, in the Gibraltar Arc (Andrieux et al., 1971; Comas et al., 1999). The Betic Cordillera is the northern branch of the arc and is formed by the External Zones, the Internal Zones, and the Flysch Trough Units between them (Fontboté & Estévez, 1980). The External Zones, located further north, are

thin-skinned thrust-and-fold systems formed due to compression of the S Iberian paleo-margin (Banks & Warburton, 1991; Meijninger & Vissers, 2007; Nebbad, 2001). They are grouped into two paleogeographical zones: the Prebetic Zone dominated by shallow facies, and the Subbetic Zone, mainly dominated by deep marine facies (García-Hernández et al., 1980). The Flysch Trough Unit consists of turbidites and clays deposited on the thinned margin and are indicators of the cordillera suture. This same Unit can be found in the eastern and central Betics, they are mainly found in the Campo de Gibraltar (Durand-Delga et al., 2000), and is deformed by thin-skinned thrust-and-fold systems and thrust over the External Zones (e.g., Luján, 2003; Luján et al., 2006). The Internal Zones, in the south and southeast, are considered to be an allochthonous terrane colliding with the paleomargin, and are formed by three main overlying metamorphic complexes and the frontal units (Fallot, 1948). At present, they have been redefined, and only the uppermost Maláguide and Alpujárride complexes are considered coming from a different continent. The Nevado-Filábride Complex, however, is considered the basement of the thinned paleo-margin that was subducted and subsequently accreted beneath the other two complexes (Booth-Rea et al., 2012, 2007; Gómez-Pugnaire et al., 2012; Platt et al., 2013).

The Betic Cordillera is formed by the NW-SE oblique convergence of the Eurasian and Nubian plates since the Late Cretaceous. In the late Oligocene, orogenic deformation starts to affect the southeastern margin of Iberia (e.g., Platt et al., 2003; Rosenbaum et al., 2002; Sanz de Galdeano, 1990; Srivastava et al., 1990). The early and middle Miocene is characterized by extensional tectonics leading to the thinning of the continental crust. The stretching involves the exhumation of the main metamorphic complexes by means of major low-angle normal faults (Aldaya et al., 1991; Crespo-Blanc, 1995; Fernández-Fernández et al., 2007; Galindo-Zaldívar et al., 1989; Jabaloy et al., 1992) and the formation of the Alborán Basin and smaller intramontane basins (Comas et al., 1999). Since the middle Miocene, compression caused uplift and the formation of large E-W to ENE-WSW antiforms (Sanz de Galdeano & Alfaro, 2004). Simultaneously, marine basins were formed in the large depressed synforms. Later, in the Late Tortonian, NW-SE fault set, together with uplift, determine the decrease in size of the Alboran Basin, and the individualization and emergence of intramontane basins (Galindo-Zaldívar et al., 2003).

Different models have been proposed to explain this evolution, and they can be separated into three groups: (a) subduction (Araña & Vegas, 1974; Pedrera et al., 2011; Ruiz-Constán et al., 2011; Wortel & Spakman, 1992; among others), (b) lithospheric delamination (Calvert et al., 2000; García-Dueñas et al., 1992; Mancilla et al., 2013; Platt & Vissers, 1989; Seber et al., 1996; among others) and, (c) slab roll-back processes (Blanco & Spakman, 1993; Booth-Rea et al., 2007; Carminati et al., 2012; Chertova et al., 2014; Faccenna et al., 2004; Rosenbaum et al., 2002; Wortel & Spakman, 2000; among others). Some delamination models suggest a slab tearing at the edges of the subduction system coeval to the slab rollback (Duggen et al., 2003; Mancilla et al., 2015; Martínez-Martínez et al., 2006; Thurner et al., 2014).

At present, the latest data indicate an oblique dextral convergence of  $4.0 \pm 0.2$  mm/yr between the Eurasian and Nubian plates, in an NNW-SSE direction (D'Acromont et al., 2014; DeMets et al., 2010; Iribarren et al., 2007). Meanwhile, a westward relative motion of the Gibraltar Arc of 3–5 mm/yr is recorded by CGPS data (Garate et al., 2015; González-Castillo et al., 2015; Palano et al., 2015; Sparacino et al., 2020; Figure 1a). In the central zone, for example, in the Granada Basin, a continuation of the E-W to ENE-WSW extension is recorded affecting mainly the internal zones, but also some regions of the external zones and their boundaries (Galindo-Zaldívar et al., 2015).

The Betic Cordillera constitutes the most seismically active region in the Iberian Peninsula. Seismicity is summed up with frequent low-moderate magnitude earthquakes concentrated mainly in upper crust (SIS, 2022; Figure 1a), intermediate depth seismicity between Alboran Sea, Málaga and Granada (Santos-Bueno et al., 2019), and rare very deep earthquakes (Buforn et al., 2011). Because of the significant along strike variations of the orogen, focal mechanisms of all types are present: normal, reverse, and strike-slip (de Vicente et al., 2008; Martín et al., 2015; Stich et al., 2003, 2010, 2006). In the central Betic Cordillera, seismicity is concentrated in the intramontane basins and dominated by normal faulting earthquakes (Galindo-Zaldívar et al., 1993, 1999; Morales et al., 1997). Seismic sequences are common in the Betic Cordillera, both in the historical and recent record (Buforn et al., 2006; Morales et al., 2015; Ocaña, 2009; Ruiz-Constán et al., 2009; Santoyo & Luzón, 2008). Regarding the central region, different sequences have been historically reported in Granada, in 1778 and 1806–1807 (Ocaña, 2009; Sempere, 1807). Recent seismic sequences include Iznájar in 1998 (Carmona et al., 2009), Loja in 1985 and 2000 (Hamdache et al., 2019; SIS, 2022), and Albuñol between 2000 and 2001 (Ocaña, 2009; SIS, 2022).



## 2.1. Granada Basin

The Granada Basin, together with the Guadix-Baza Basin, are the biggest intramontane basins of the Betic Cordillera. The Granada Basin is located in the central region, bounded on the E-SE side by the highest areas of the mountain range, the Sierra Nevada. In the early Miocene, the western border of Sierra Nevada (Figure 1) was affected by ENE-WSW extension. The Granada Basin (Figure 1b) begins to form in this period, shown by the Burdigalian oldest continental sediments lying only on top of the Alpujarride Complex (Braga et al., 1990). Main NW-SE to NNW-SSE normal faults (Sanz de Galdeano et al., 2001) led to the individualization of the Granada Basin in the late Tortonian. In this period, marine sediments were deposited (Rivas et al., 1999) over the Subbetic Zone basement in the N-NW half, and over the Alpujarride Complex in the S-SE half. These faults sink the Granada Basin with respect to the uplifted Sierra Nevada and Sierra Arana, generating the main depocenters (Rodríguez-Fernández & Sanz de Galdeano, 2006). In the late Tortonian, the regional uplift isolated the Granada Basin from the Mediterranean Sea depositing evaporitic materials and later continental sediments (García-Alix et al., 2008). During the Pliocene, alluvial fan systems were deposited at the feet of Sierra Nevada, Sierra Arana and Sierra Tejada. In the Quaternary, the deposition and subsidence concentrated in the northern and eastern parts of the basin (Galindo-Zaldívar et al., 2015; García-Alix et al., 2009; Morales et al., 1990; Rodríguez-Fernández & Sanz de Galdeano, 2006; Ruano et al., 2004). Finally, since the early Pleistocene, the basin was captured by the Guadalquivir Basin (García-Alix et al., 2009).

The Granada high-angle normal fault sets have been related to the Mecina detachment, the low-angle normal fault that exhumed Sierra Nevada (Galindo-Zaldívar et al., 1991, 1996; Jabaloy et al., 1993), and has been recently considered the active section of the same extensional system (Madarieta-Txurruka et al., 2021). The NW-SE to NNW-SSE high-angle normal faults are considered to be active (García-Mayordomo & Martín-Banda, 2022) and generate continuous moderate seismicity reaching Mw 4.5 earthquakes (Sanz de Galdeano & Peláez, 2011). Detailed analysis of the focal mechanisms in the Granada Basin also suggests a relationship between earthquakes of up to Mw 4.0 and low-angle normal faults (Madarieta-Txurruka et al., 2021). The main faults of the basin have slip rates ranging from 0.05 mm/yr to more than 0.25 mm/yr, calculated by geological data (Sanz de Galdeano et al., 2003). Recent high-precision leveling data suggest higher slip rates for the Granada Fault, about 1 mm/yr (Madarieta-Txurruka et al., 2021).

## 2.2. Sierra Elvira

Sierra Elvira is the main horst of the basement within the Granada Basin (Figures 1b and 2). It is formed by Mesozoic rocks of the Subbetic Zone, from the Carnian to the Berriacian (Braga et al., 1979; García-Dueñas, 1967). The older structures, affecting only the Mesozoic series, are compressional. Western Sierra Elvira is affected by NE-SW south-vergent inverted folds and N70°E trending thrusts. These structures are related to the last stage of the transgressive phase between External and Internal zones during the early-middle Miocene. The thrust is related to an extrusion of Triassic evaporites with subvolcanic rocks (ophites; Lupiani & Soria, 1988). Sierra Elvira can be divided into two areas: (a) Western Sierra Elvira, with higher elevations and affected by folds, and (b) eastern Sierra Elvira, with a lower elevation, affected by thrusts and including outcrops of evaporites. The Subbetic outcrop is completely surrounded by Pliocene-Quaternary deposits due to the activity of NE-SW and NW-SE normal faults since the latest Miocene, which is responsible for the formation of large fault scarps on the SE and SW edges (Lupiani & Soria, 1988). The NW-SE set is considered active (García-Mayordomo & Martín-Banda, 2022).

## 3. Methodology

### 3.1. Geology

New field geology data have been acquired in order to understand the structure and kinematics of the faults, and their relationship with recent sediments. This new data was then used to update the available geological maps (Figures 2 and 3).

The Granada 2021 seismic sequence is located at the S-SW of Sierra Elvira (Figure 1b). This outcrop of Mesozoic rocks is the main uplifted basement block in the Granada basin and is closely related to the activity of the main faults. We propose that the Sierra Elvira sector could have the same characteristics as the basement zones

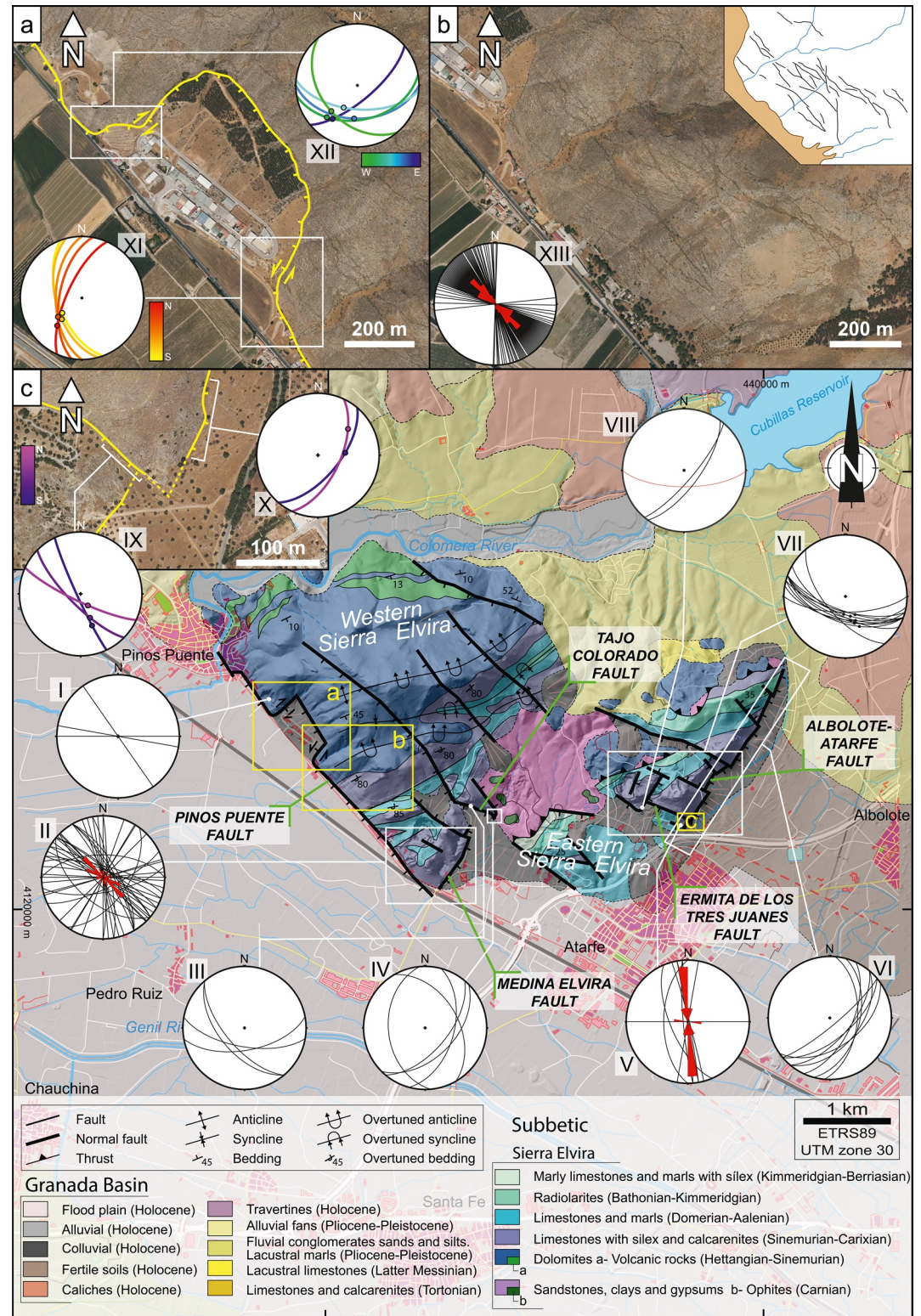


**Figure 2.** Geological map of Sierra Elvira and surrounding areas. Updated from Lupiani & Soria (1988). Stereonets (Schmidt net, lower hemisphere) of the fault sets and joints of Sierra Elvira are shown. (a) Detail of the “tooth-shaped” Pinos Puente Fault in Western Sierra Elvira. (b) Detail of the fractures in the SW edge of Western Sierra Elvira. (c) NW-SE and NE-SW fault set intersection in Eastern Sierra Elvira.





**Figure 3.** Field observations. (a) Recent joints affecting Quaternary sediment in the S border of Western Sierra Elvira. (b) Normal fault in the SE of the Eastern Sierra Elvira. (c) Striae in the fault surface indicate normal to left-lateral behavior. (d) Ermita de los Tres Juanes Fault plane. (e) Tajo Colorado Fault scarp. (f) Striae on the fault plane indicate a normal behavior of the Tajo Colorado Fault. (g) Pinos Puente Fault in the SW border of Western Sierra Elvira with striae suggesting normal movement. (h) Striae indicating normal to right-lateral kinematics in Pinos Puente Fault. (i) Quarries in SE of Western Sierra Elvira. The area is extensively fractured, with faults and joints. (j) Tensional joint striking N135°E filled by carbonates at different stages of precipitation. (k) Tensional joint striking N165°E with an opening of up to 3 m, near the intersection between the Medina Elvira and the Pinos Puente faults.

affected by the seismicity at 3–5 km depth. Therefore, the fractures of Sierra Elvira have been studied, analyzing the main sets of joints by means of detailed fieldwork and satellite imagery. The obtained data made it possible to understand the recent stress regimes and the activity of the structures.

### 3.2. Gravity Methods

Gravity methods are very useful when studying sedimentary basins. The sedimentary fill contrasts with the basement because of its lower density and, consequently, presents gravity anomaly minima that are used to determine the geometry of the basement. The existence of faults at depth produces abrupt variations in the thickness of the sedimentary infill and therefore, can be identified in the gravity anomaly maps.

This study includes the reprocessing of gravity data available for the Granada Basin and its immediate vicinity (Figure 4). The database comprises: (a) data collected in the TopoIberia project (Ayala et al., 2016; SIGEOF, 2022), (b) data published by Madarieta-Txurruka et al. (2021), and (c) new data obtained in the SE of the basin. The processing begins with the leveling of the different surveys. Then, Free Air, Bouguer, and Terrain corrections were applied to obtain the Complete Bouguer Anomaly for each station, using a standard density of



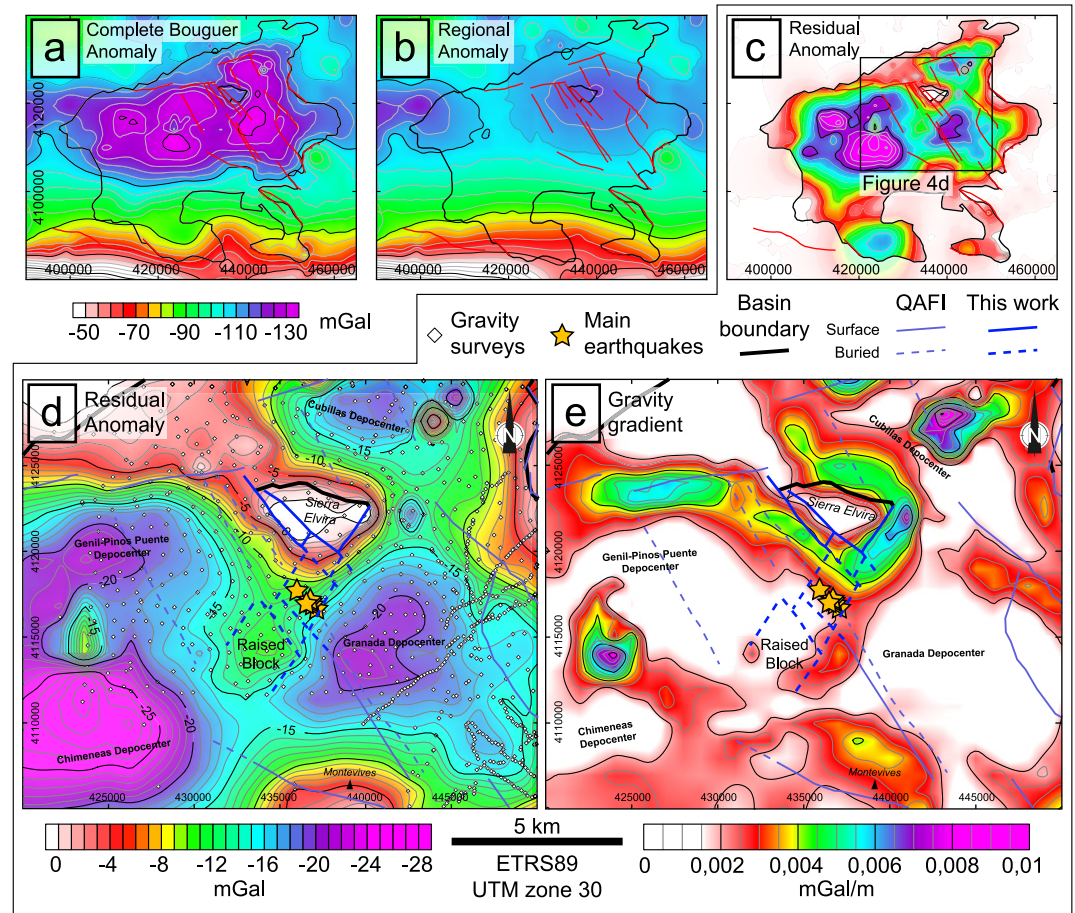


**Figure 4.** Gravity anomaly maps of the Granada Basin and the 2021 seismic sequence area. (a) Complete Bouguer Anomaly. (b) Regional anomaly. (c, d) Residual anomaly. (e) Gravity gradient. Faults related to the Granada 2021 seismic sequence are indicated in dark blue and faults recompiled in the QAFI database (García-Mayordomo & Martín-Banda, 2022; QAFI, 2022) are indicated in light blue.

2.67 g/cm<sup>3</sup>. The Terrain Correction process was computed combining Kane (1962) and Nagy (1966) methods, using a 5 m pixel resolution DTM developed by the Spanish Instituto Geográfico Nacional (IGN; CNIG, 2022), up to a distance of 20 km from the sites (Fullea et al., 2008).

The reprocessed data were used in the construction of a new Complete Bouguer Anomaly map of the Granada Basin (Figure 4a) using *kriging*. However, an adequate characterization of the basin requires a residual anomaly map, which is obtained by extracting the regional anomaly. Several methods were considered for the calculation of the regional and residual gravity anomalies: (a) polynomial fitting (first- second- and third-order), (b) Fast Fourier Transformation-Gaussian Regional/Residual Filter (standard deviation of 0.15, 0.18 and 0.2), and (c) using only data measured outside the basin. Finally, it was calculated using only the data obtained outside the basin, because that was the method that best fitted the 0 values of residual anomaly with the basin boundary (Figures 4b and 4c). In addition to the residual gravity anomaly map of the Granada Basin, another map of the area affected by the 2021 seismic sequence was obtained (Figure 4d). Going further in the gravity analysis in order to locate abrupt changes in the gravity signal, and applying this to detect major boundaries/faults (Blakely, 1996; Grauch & Cordell, 1987), we have obtained the horizontal gradient of the residual anomaly map (Figure 4e) using the two orthogonal horizontal, *x* and *y*, derivatives as follows:

$$HG(x, y) = \sqrt{\left(\frac{\partial \Delta}{\partial x}\right)^2 + \left(\frac{\partial \Delta}{\partial y}\right)^2} \quad (1)$$



where  $\Delta$  represents the value of the residual gravity anomaly, and HG is the value of the horizontal gravity gradient.

### 3.3. Seismicity

The seismic data collected by the National Seismic Network of the Spanish IGN were compiled in this study (Figures 5a and 6a and Table 2). Using the Thatcher and Hanks (1973) approximated relationship between local magnitude and seismic moment, a total estimated released seismic moment was obtained (Figure 6b). In addition, the magnitude distribution of seismic activity was studied using the Gutenberg-Richter power law (Gutenberg & Richter, 1944). From the plot of the log of the cumulative number of earthquakes vs. magnitude, a  $b$ -value (slope of the lineal fit) was estimated (Figure 6c). The  $b$ -value is a critical parameter in seismic hazard studies, because it reveals the large to small earthquakes rate in the sequence. Its value is dependent in some way on the tectonic setting of the area (Lee & Yang, 2006).

The focal mechanism solutions for the largest earthquakes recorded in January 2021 (Table 3) were computed by the Spanish IGN (SMT, 2022), using the Rueda and Mezcuca (2005) approach (Figure 5b). Finally, the reduced stress tensor (Figure 6d) was computed using the inversion approach developed by Delvaux and Barth (2010) and Delvaux and Sperner (2003) with the Win-Tensor™ code.

#### 3.3.1. Relocation of the Seismicity

The seismicity directly recorded by the Spanish IGN shows a typical “spot-shaped” pattern (Figure 5a) that is due to the uncertainties involved with any location processing method. For this reason, it was necessary to relocate events in order to improve the locations, particularly the relative locations among events. The HypoDD code (Waldhauser, 2001; Waldhauser & Ellsworth, 2000) was used for this goal, a software based in the so called double-difference earthquake location algorithm, enhancing relative locations of events. Absolute locations, on the other hand, strongly depend on the reliability of the shear velocity model used (Waldhauser & Richards, 2004). In previous works, the same approach and code were used in the same regions, and regions nearby (Marín-Lechado et al., 2017; Morales et al., 2015; Tendero-Salmerón et al., 2020).

The P and S phase data recorded by the IGN were used for the process, coming from the permanent seismic net, the permanent accelerometer net, and also two non-permanent seismic stations deployed by the IGN on 25 January 2021, in order to improve locations and provide a better azimuthal coverage of the sequence.

Different data sets, parameters, and shear velocity models have been tested, trying to obtain the smallest errors. Only earthquakes above magnitude  $m_{bLg}$  1.5 were considered in the relocation, in order to better determine the arrival time of phases. S phases from acceleration records have not been considered, due to the uncertainty in its picking. In addition, only earthquakes recorded in more than eight stations, and only differences among event couples with 12 records were included, being the distance between the event couple and the station less than 150 km. Concerning the used shear velocity model, after some tests, the Palomeras et al. (2014) model was selected, even though the observed differences with the results obtained with the regional IGN model (Table 1) were not noticeable.

Following these rules, more than 770 events were relocated (Figure 5b), with a mean error somewhat below 1 km, both in location and depth. Several of these relocated earthquakes did not have a depth value assigned in the initial location process conducted by the IGN. This is because the error in the computed depths was above 5 km, in mostly cases.

The relocation of the seismic sequence made it possible to define more precisely the Subsurface Rupture Length (SbRL) and the RA. In this way, the expected magnitude for an earthquake occurring in the proposed segment ( $M_{segment}$ ) and the expected seismic moment for the segment ( $M_0$ ) can be estimated in order to compare them with real data. For this purpose, the RA is evaluated by multiplying SbRL with rupture width (RW; Wells & Coppersmith, 1994). RW will be obtained by  $D/\sin(\delta)$  (Wesnousky, 2008), being  $D$  the depth of the seismic zone and  $\delta$  the dip of the faults.

$M_0$  can be obtained using the formulas proposed by Leonard (2010) for down-dip faults.

$$\log(M_0) = 6.10 + 1.5 * \log(RA) \quad (2)$$

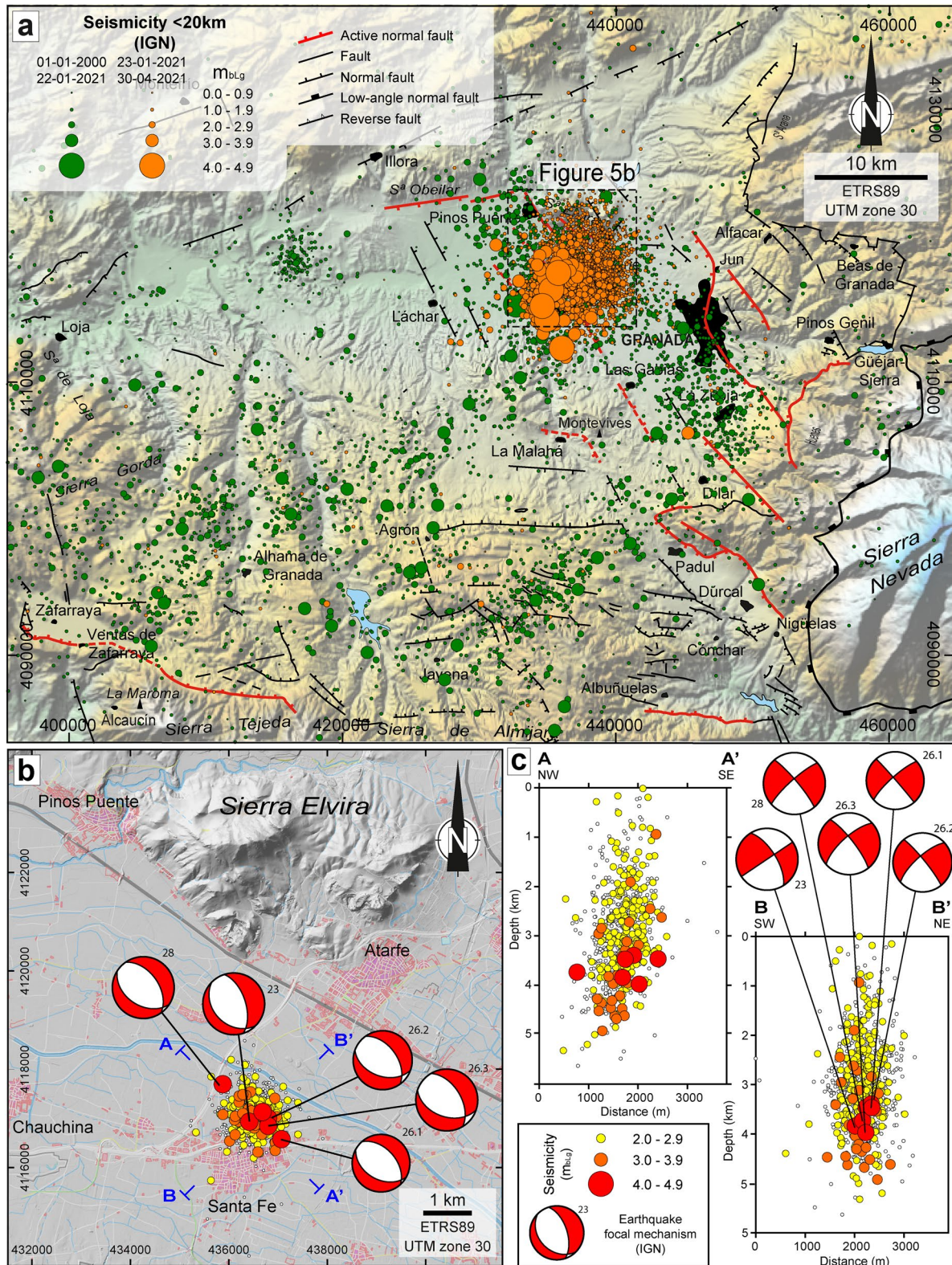


**Figure 5.** Granada 2021 seismic sequence. (a) Topographic map of the Granada Basin with seismicity provided by the Spanish IGN (SIS, 2022). In orange, the seismicity related to the 2021 seismic sequence. (b) Topographic map of the Sierra Elvira and Santa Fe area, with the relocation of the 2021 seismic sequence and available earthquake focal mechanism data (Table 3). (c) Projected NW-SE and NE-SW cross sections of the 2021 seismic sequence and rotated earthquake focal mechanisms.



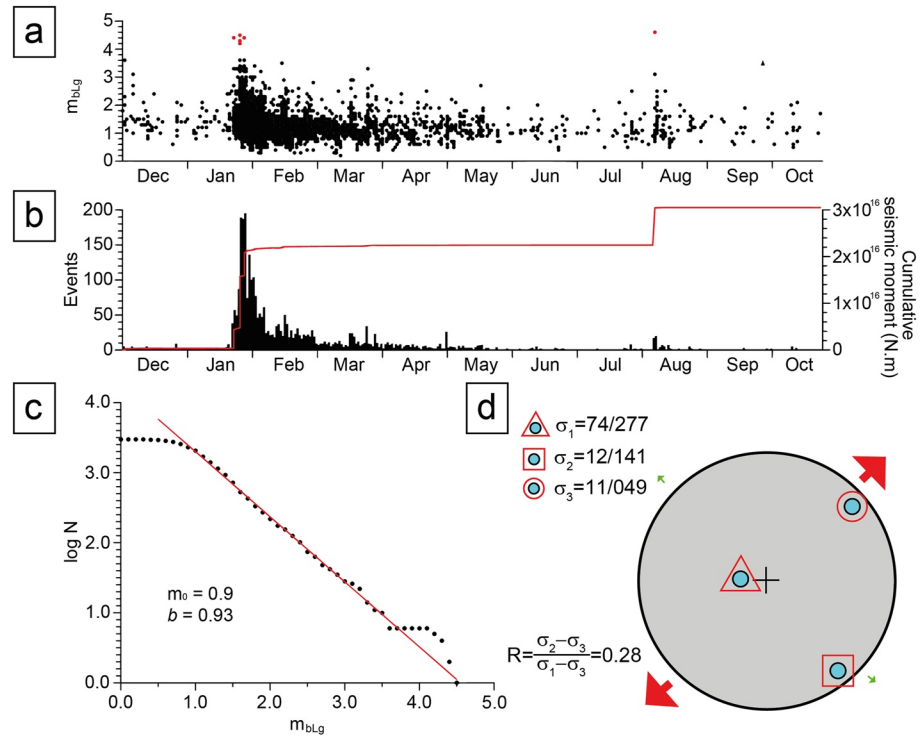


**Figure 6.** Seismicity during December 2020 to October 2021 time interval. (a) Behavior of the sequence. (b) Daily number of recorded earthquakes and cumulative seismic moment. (c) Plot of the log of the cumulative number of earthquakes vs. magnitude. The linear fit is shown. (d) Reduced stress tensor of the sequence derived from earthquake focal mechanism.

$$\log(M_0) = 6.10 + 3.0 * \log(\text{SbRL}) \quad (3)$$

To estimate the magnitude that a single earthquake would have for these parameters, the following formulas proposed for normal faults by Wells and Coppersmith (1994) will be used, since they allow comparing both the RA and the SbRL with the Mw.

$$Mw = 3.93 + 1.02 * \log(\text{RA}) \quad (4)$$

$$Mw = 4.34 + 1.54 * \log(\text{SbRL}) \quad (5)$$

In addition, the moment magnitude is obtained from the  $M_0$  value calculated in Equations 2 and 3 from the well-known relationship (Hanks & Kanamori, 1979):

$$Mw = \frac{2}{3} \log(M_0) - 6.07 \quad (6)$$

**Table 1**  
Shear Velocity Models Used in the Relocation Process

IGN model		Palomeras et al. (2014) model	
Depth (km)	$V_S$ (km/s)	Depth (km)	$V_S$ (km/s)
0–11	3.49	0–5	3.10
11–24	3.66	5–15	3.40
24–31	3.94	15–25	3.65
>31	4.57	25–30	3.85
		30–35	4.10
		35–45	4.30
		45–50	4.42
		50–75	4.45

### 3.4. CGPS Data Processing

In 2008, a CGPS network was established to monitor crustal deformation in Spain and Northern Morocco (Galindo-Zaldívar et al., 2015; Garate et al., 2015; González-Castillo et al., 2015). LOJA, PALM, and NEVA are the sites used in this work that belongs to the central sector of Betic Cordillera (Southern Spain). The monuments that host the CGPS points of these sites are founded on bedrocks, which implies a strong stability of the concrete pillars and, therefore, a high quality of GPS data. The GPS data time span considered was since March 2008 up to December 2019. The data were processed

**Table 2**  
Recorded Events With Magnitude Above  $m_{bLg}$  4.0

Date	Time (hh:mm:ss)	Depth (km)	$m_{bLg}$	Mw	Intensity
23 January 2021	11:15:24	3	4.4	4.4	V–VI
26 January 2021	21:36:33	5	4.2	4.1	V
26 January 2021	21:44:18	5	4.3	4.2	V
26 January 2021	21:54:55	5	4.5	4.4	V–VI
28 January 2021	18:49:49	5	4.4	4.4	V
12 August 2021	21:25:12	-	4.6	4.5	V

Note. Data shared by the Spanish IGN (SIS, 2022).

using GipsyX, software developed at the Jet Propulsion Laboratory (Bertiger et al., 2020). The processing method used was the precise point positioning. Once all the site's coordinates were computed in the IGS14 reference frame, we created the position time series in North and East components and estimated the absolute velocities. A more effective representation of the velocity field was estimated through the residual velocities with respect to stable Eurasia (Figure 7 and Table 4). Additionally, we computed residual velocity vectors with respect to site NEVA (Figure 7 and Table 4), allowing to further analyze the shallow deformation and extension in the Granada Basin.

## 4. Results

### 4.1. Structure of the Central Granada Basin

#### 4.1.1. Geological Data

The area affected by the seismicity of the 2021 sequence is located near Sierra Elvira, the main Subbetic basement outcrop in the Granada Basin (Figure 2).

The most recent structures are extensional, and they divide Sierra Elvira into two areas, affecting very recent sediments (Figure 3a). The main structures are two sets of normal faults striking NE-SW and NW-SE (Figure 2). In the NE-SW set, there are two main faults, the Medina Elvira and Albolote-Atarfe faults. The Medina Elvira Fault (Figure 2) is located at the boundary between Western and Eastern Sierra Elvira, and it strikes N30°E, dipping to the SE. Although scarps are observed only in a segment of the fault, their continuity can be discerned from the geological and geomorphological analysis. In the SW, the Medina Elvira Fault separates the Jurassic series from the Quaternary deposits of the Granada Basin, while to the NE it is cut by the Tajo Colorado Fault and further on it is difficult to follow its trend because it is covered by evaporites (Figure 2). However, the presence of structurally higher Subbetic rocks in the SE, rather than in the NW, points to the presence of a normal fault. The Albolote-Atarfe Fault is the other main fault of this set and it limits the Eastern Sierra Elvira to the SE (Figure 3b). It has an average strike of N035°E and an average dip of 55°SE (Figure 2; Stereonet VI). It is segmented and slightly displaced by the NW-SE fault set. The striae of the Albolote-Atarfe Fault indicate a normal to left-lateral movement, becoming more left-lateral to the NE (Figures 2c and 3c; Stereonet X). There are more small faults of this set, such as the one cutting the Ermita de los Tres Juanes Fault, striking N138°E and dipping 70°SE (Figure 2; Stereonet VIII).

The NW-SE set is formed by the Ermita de los Tres Juanes, Pinos Puente, and Tajo Colorado faults with preserved scarps, and other smaller or no-scarp faults. The Ermita de los Tres Juanes Fault is located in Eastern Sierra Elvira and has a well-preserved scarp (Figure 3d), striking N115°E and dipping 67°SW (Figure 2; Stereonet VII). The striae indicate a normal to left-lateral movement of the fault (average rake of 72°SE). In the southeastern termination, it strikes N145°E, dips an average of 80°SW and the striae suggest more left-lateral behavior, reaching a rake of 45°SE (Figure 2c; Stereonet IX). To the northwest, the Ermita de los Tres Juanes Fault is cut by a minor fault and is displaced toward the SW. The Tajo Colorado Fault (also called Atarfe Fault, Sanz de Galdeano et al., 2003) is located to the W, and it affects both the western and eastern Sierra Elvira. It has an average strike of N134°E and an average dip of 60°SW (Figures 2 and 3e; Stereonet III). The striae and other kinematic indicators suggest an average normal slip (Figure 3f). In the southeastern termination, reaching the Carnian evaporites,

**Table 3**  
Solutions for Shallow Earthquake Focal Mechanisms Represented in Figure 5b Computed by the Spanish IGN (SMT, 2022)

N	Date	Time (hh:mm:ss)	Long. (°E)	Lat. (°N)	Depth (km)	Magnitude (Mw)	Strike (°)	Dip (°)	Rake (°)	CLVD
23	23 January 2021	11:15:24	-3.7239	37.2062	3	4.4	342	59	-75	0.09
26.1	26 January 2021	21:36:33	-3.7296	37.1951	5	4.1	318	49	-77	0.07
26.2	26 January 2021	21:44:18	-3.7330	37.1756	5	4.2	324	51	-67	0.16
26.3	26 January 2021	21:54:55	-3.7369	37.1843	5	4.4	329	53	-63	0.02
28	28 January 2021	18:49:49	-3.7206	37.1565	5	4.4	325	50	-75	0.02

Note. N: corresponds to the numbers in Figures 5b and 5c. CLVD: adjustment of the focal mechanism inversion indicated in the Compensated Linear Vector Dipole.



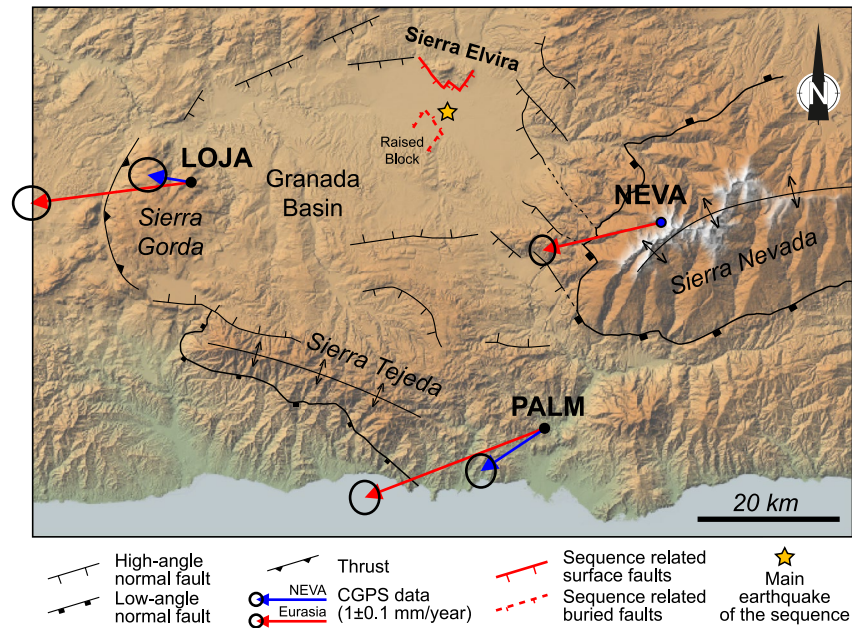


**Figure 7.** Topographic map with continuous GPS (CGPS) data and main recent faults. Residual velocity field with respect to the Eurasia fixed reference frame (red arrows) and respect to stable NEVA (blue arrows) and 95% confidence ellipses.

the Tajo Colorado Fault has a “horsetail-shape” striking roughly N-S, and fault planes dips to the W and E-SE (Figure 2; Stereonet IV). It probably continues in the SW of the evaporites, where there is an important topographic discontinuity with the same strike. The Pinos Puente Fault (Sanz de Galdeano et al., 2003) is located at the SW boundary of the Western Sierra Elvira. It has an average strike of N140°E and an average dip of 60°SW. It has a remarkable scarp and average striae with normal to right-lateral movements (Rodríguez-Fernández & Sanz de Galdeano, 2006; Sanz de Galdeano et al., 2012). The fault plane locally displays a “tooth-shaped” curvature (Figure 2a). It seems that in this sector the NE-SW fault set cuts the Pinos Puente Fault. However, if we look at the intersections (Stereonet XI and XII), it is observed that the fault bends to reach N020°E at the SE intersection, and N050°E at the NW intersection. In addition, the striae suggest a displacement to the SW of the hanging wall block in all the segments of the fault: (a) normal behavior in the N140°E segments (Figure 3g), (b) normal to left-lateral behavior in the N025°E segment (Stereonet XI), and (c) normal to right-lateral behavior in the N050°E segment (Stereonet XII; Figure 3h). Something similar happens between the Ermita de los Tres Juanes Fault and a NE-SW fault that cuts it. At the NE intersection, the NE-SW fault cuts the Ermita de los Tres Juanes Fault. At the SW intersection, however, the NE-SW fault bends reaching N140°E strike (Figure 2; Stereonet VIII). The rest of the faults of this set do not have an important scarp, or are smaller. They have an average strike of N140°E and are mainly dipping to the SW.

Focusing on the intersections between the two major sets of faults, we can summarize the following: (a) mainly the NW-SE fault set cuts the NE-SW fault set, the opposite scarcely occurs (Figure 2). (b) In some intersections, there is no fault segmentation, but there is a bending until reaching the strike of the other set of faults (Stereonet XI and XII). (c) The striae change as we approach the endings of each segment, in some cases intensifying the normal behavior, and in other cases the strike-slip kinematics (Stereonet IX and X).

**Table 4**

*East and North Residual Velocities With Respect to the Eurasia Fixed Reference Frame and Respect to Stable NEVA*

Sites	Coordinates		Residual velocities (mm/yr) stable Eurasia				Residual velocities (mm/yr) stable NEVA			
	Long. (°E)	Lat. (°N)	VE	σE	VN	σN	VE	σE	VN	σN
LOJA	-4.1064	37.1073	-2.3	±0.29	-0.3	±0.26	-0.6	±0.29	0.1	±0.26
NEVA	-3.3856	37.0626	-1.7	±0.2	-0.4	±0.23	0.0	-	0.0	-
PALM	-3.5623	36.8090	-2.6	±0.23	-1.0	±0.26	-0.9	±0.23	-0.6	±0.26

In addition to normal faults, there are other extensional structures. The massif is fractured by different families of joints. The brittle deformation becomes more pronounced to the S, at the intersection of main faults (Figures 2 and 3i; Stereonets II, V, and XIII). The area where the Pinos Puente and Medina Elvira faults intersect, in Western Sierra Elvira, is the most fractured one. There are joints striking in all directions, but predominantly, they have strikes of N110°–140°E, mainly between N130°E and 140°E (Stereonet II). Some of them affect Quaternary sediments (Figure 3a). The joints with larger openings can reach up to 3 m (Figure 3k) and the strike ranges between N120°E and 165°E. Some joints are filled with decimetrical boulders. In addition, in several of them, carbonates are precipitated. Figure 3j shows different precipitation phases in a joint. The first grows in layers parallel to the joint walls, reaching thicknesses of 10 cm in each wall (in green). The second grows perpendicular to the joints, filling the opening of the second phase, up to 15 cm (in red). To the NE, before the “tooth-shaped” curvature of the Pinos Puente Fault, there are fractures visible in satellite imagery (Figure 2b). Most of the joints strike between N110°E and N150°E, predominantly N130°–140°E (Stereonet XIII). No joints are observed striking NE–SW, but there could be, although with small aperture and not visible in the orthophotos. In the western border of Sierra Elvira, the number of fractures decrease and the existing joints strike from N090°E to N145°E (Stereonet I).

In the eastern Sierra Elvira, fractures are not as many as in the Western Sierra Elvira. The data obtained in the intersection zone of the Albolote-Atarfe and Ermita de los Tres Juanes faults suggest an extended fragmentation, but one that only shows centimeter-size openings. In addition, the data indicate a predominance of the N–S strike (Stereonet V).

#### 4.1.2. Gravity Data

The Complete Bouguer Anomaly map (Figure 4a) shows a minimum in the Granada Basin. The values in this region are generally below  $-120$  mGal and reach  $-138$  mGal. Toward the north and the south, the values increase, reaching the highest values, up to  $-50$  mGal, in the southern part of the study area. This regional increase of the Complete Bouguer Anomaly values is due to long-wavelength anomalies, and therefore, probably related to the crustal thickness. The regional gravity anomaly map allows a better observation of reported anomalies (Figure 4b). It shows minimum values in Sierra Elvira and in the NE of the Granada basin, reaching  $-124$  mGal. Values of  $-50$  mGal are again found in the southern part of the study area.

The residual gravity anomaly map offers a better recognition of the basin structure and of the area affected by the seismic sequence (Figures 4c and 4d). Four depocenters can be distinguished from the anomaly minima. These depocenters coincide with those described by Madarieta-Txurruka et al. (2021), Morales et al. (1990), Rodríguez-Fernández, and Sanz de Galdeano (2006). With respect to the map in Figure 4d, the Cubillas depocenter, located to the NE, reaches  $-19.5$  mGal. The Granada Depocenter is located in the SE, with values up to  $-21$  mGal. In the NW, the Genil-Pinos Puente Depocenter reaches values of  $-22$  mGal, and the Chimeneas Depocenter is located in the SW, with the minimum residual values of the basin, reaching  $-29$  mGal. The maximum values of the residual gravity anomaly, close to 0 mGal, are observed at the basin limits and in Sierra Elvira. The eastern and western depocenters are separated by Sierra Elvira and a relative maximum with a “rhomboid-shape” and values between 0 and  $-15$  mGal.

Three of the described depocenters surround Sierra Elvira: Cubillas to the NE, Granada to the SE and Genil-Pinos Puente to the W (Figure 4d). High gradient values between 0.004 and 0.008 mGal/m are observed at the former boundaries (Figure 4e). The high gradients S to Sierra Elvira (0.003 mGal/m) are also remarkable, in accordance with the “rhomboid-shaped” relative maximum (Figure 4d). Other zones with remarkable gravity gradients are observed in the map: (a) two points with values higher than 0.01 mGal/m in the Cubillas Depocenter, and between the Chimeneas and Genil-Pinos Puente Depocenters. (b) E–W lineation up to 0.006 mGal/m north of the Genil-Pinos Puente Depocenter. (c) NW–SE lineations between 0.003 and 0.005 mGal/m next to the Montevives mine and to the NE of the Granada Depocenter.

#### 4.2. Granada 2021 Seismic Sequence

This seismic sequence is located in an area (Figure 5a) with a sustained level of very low to low magnitude events (Madarieta-Txurruka et al., 2021). In December 2020, this level increased, and from December 2020 to November 2021 near 3,000 events have been recorded by the Spanish IGN, although nearly 1100 of them have no depth assigned.



The sequence consists of two superimposed phases (Figures 6a and 6b). Initially, the number of events suddenly increased in the area, reaching a level of nearly 200 recorded events per day in a period of three days at the end of January. In this phase, five earthquakes above magnitude  $m_{bLg}$  4.0 happen, all of them felt by the population with intensity V or V–VI (Table 2; EMS-98 scale; Grünthal, 1998). Three of these earthquakes happened on the 26th of January, in less than 20 min. After a gradual decay in the recorded magnitudes and number of earthquakes per day for more than six months, on August 2021, a second phase including the most energetic earthquake of the sequence was recorded. It was an event with magnitude  $m_{bLg}$  4.6, felt with intensity V and not accompanied by a significant level of seismicity, in this case. Starting from that event, a new decay in the level of seismicity and recorded magnitudes was observed. In addition to these five earthquakes above magnitude  $m_{bLg}$  4.0, other 29 events in the range of  $m_{bLg}$  3.0–4.0 were recorded.

A total estimated released seismic moment of  $3.0 \times 10^{16}$  N-m was obtained (Figure 6b). The phases had an estimated seismic moment of  $2.25 \times 10^{16}$  N-m and  $0.75 \times 10^{16}$  N-m, equivalent to an earthquake of Mw 4.8 and Mw 4.5, respectively. A  $b$ -value equal to 0.93 ( $\sigma = 0.02$ ) is a typical value (Figure 6c), close to the unit, obtained in many other seismic sequences in the Ibero-Maghrebian region (Hamdache et al., 2019) and conventional mainshock-aftershock sequences (Frohlich & Davis, 1993). Furthermore, from the plot, it can be clearly seen that the sequence can be considered complete above magnitude  $m_{bLg}$  0.9 (threshold magnitude), from which the linear behavior is observed, that is, the vast majority of events above this magnitude were recorded by the IGN seismic net.

The focal mechanism solutions for the largest earthquakes (Figure 5b and Table 3) show a clear extensional pattern, also revealed when computing the reduced stress tensor of the sequence from them. It depicts an NE-SW horizontal extension and a near vertical compression, with an axial ratio of  $R = 0.28$  (Figure 6d).

#### 4.2.1. Relocation of the Seismicity

The relocation of seismic data has provided more accurate locations for earthquakes for the 2021 seismic sequence with magnitudes higher than  $m_{bLg}$  1.5. As a result, we can conclude that most of the events are located in an area no bigger than 4 km<sup>2</sup> in the N-NE of Santa Fe (Figure 5b). The six earthquakes with magnitudes above Mw 4.0 are aligned in an NW-SE direction, parallel to the principal seismogenic faults of the region (i.e., Pinos Puente Fault, Tajo Colorado Fault; García-Mayordomo & Martín-Banda, 2022).

At depth (Figure 5c), the seismic sequence present a “chimney-shape” between 5 and 0 km. It has a planarity of 0.1, calculated from the formula provided by Vidale (1986), which is a very low value for vertical seismic sequences (Vidale et al., 2006; Vidale & Shearer, 2006). Seismicity below 5 km is near to non-existent. Most earthquakes are concentrated within 3–5 km depth, being the zone where most of  $m_{bLg} > 3$  earthquakes are located. Those greater than  $m_{bLg}$  4.0 are located between 3 and 4 km depth. Above 3 km, the observed seismicity decreases both in quantity and magnitude up to the surface.

#### 4.3. Regional CGPS Data

The three CGPS sites, located in the central Betic Cordillera, have provided horizontal velocities surrounding the Granada Basin. All of them move toward the W-WSW, with respect to stable Eurasia, with horizontal velocity rates between 1.5 and 3 mm/yr (Figure 7; Table 4). NEVA is located in Sierra Nevada, to the E of the Granada Basin, and is the site with the lowest rates ( $1.7 \pm 0.2$  mm/yr to the W). In Sierra Gorda, to the W of the Granada Basin, the LOJA site presents similar direction but higher displacement rates ( $2.3 \pm 0.3$  mm/yr). Finally, in the south of Granada Basin, PALM shows the highest rates ( $2.8 \pm 0.25$  mm/yr) to the WSW. If we consider Sierra Nevada and the NEVA site stable (Figure 7), LOJA shows  $0.6 \pm 0.1$  mm/yr rates to the W-WNW and PALM presents velocity rates of  $1.1 \pm 0.1$  mm/yr to the SW.

### 5. Discussion

Multidisciplinary studies combining geological, geophysical, and geodetic data are of essential importance to study the active tectonics and recent evolution in the Alpine Cordilleras. The collision between the Eurasian and Nubian plates raises the Betic Cordillera (Braga et al., 2003; Reinhardt et al., 2007; Sanz de Galdeano & Alfaro, 2004), while it is affected by extensional processes in the neighboring Granada Basin and Sierra Nevada (Galindo-Zaldívar et al., 1999). Normal faults derived from this tectonic activity are responsible for the seismicity

affecting the region. Moderate seismic activity is common in the region (Sanz de Galdeano et al., 2003), and it can be intensified by seismic sequences, such as the one that occurred in the beginning of 2021 in Santa Fe, Granada. Geological field data and gravity analysis have made it possible to establish the structure of the Sierra Elvira uplifted massif and that of the sector below the Granada Basin. The improved location of the 2021 seismic sequence helps to link the seismicity to specific tectonic structures. The combination of fault orientation, fault kinematic data, focal mechanism, and regional CGPS data, make it possible to frame the Granada 2021 seismic sequence in the active evolution of the central Betic Cordillera.

### 5.1. Structure of the Area Affected by the 2021 Seismic Sequence

Field geology data and detailed gravity analysis in the sector affected by the sequence suggest a great brittle deformation of the basement, and the presence of two main fault sets striking N20°–40°E and N100°–140°E. The two sets of faults affect both the uplifted Sierra Elvira massif (Figures 2 and 3) and the basement under the Granada Basin. The local residual gravity anomaly map (Figure 4d) shows a “rhomboid-shape” relative maximum at the S-SW of Sierra Elvira. The data points to the existence of a raised block in that area (Figures 4d and 4e). The directions of the boundaries of this raised block, especially the eastern ones, coincide with those of the two main sets of faults.

The main dip direction of the NW-SE set of faults observed in the field is to the SW, and for the NE-SW set, it is to the SE. However, we suggest the existence of NW- and NE-dipping faults to explain the uplift of the “raised block” with respect to the Genil-Pinos Puente and Granada depocenters (Figure 8a). In fact, there are examples of NE-dipping faults in Sierra Elvira (Figure 2) or observed in seismic profiles (Santa Fe Fault; Sanz de Galdeano et al., 2010). Previous studies for the sector, based mainly on seismic profiles but also in gravity data, suggested the existence of a single fault set. Morales et al. (1990) emphasize a main fault set of N030°E direction cutting NW-SE faults located further to the NW. On the contrary, for Rodríguez-Fernández and Sanz de Galdeano (2006), the NW-SE set of faults is dominant, starting in Sierra Elvira and crossing the Granada Depocenter. Our model suggests that both fault sets determine the shape of the basement in the central part of the Granada Basin and we propose a two-directed horst and graben system (Figure 8).

The interaction between the two sets of faults is complex. In a general sense, the NW-SE set mostly cuts the NE-SW one; however, there are cases where the opposite occurs (Figure 2). In addition, at some intersections, the fault surface bends instead of being cut by another plane (Figure 2a; Stereonet VII). These data suggest that both sets of faults must have been active recently, although the activity of the NW-SE set predominates. In addition to the major fault sets, Sierra Elvira is highly fractured by smaller high-angle faults and vertical joints. The main direction of the tensional joints is NW-SE (Figure 2), coinciding with one of the main fault sets and with the extension registered in the central Betic Cordillera (Galindo-Zaldívar et al., 1993; Stich et al., 2006).

#### 5.1.1. Intense Brittle Deformation as a Result of the Recent Evolution of the Central Betic Cordillera

The central Granada Basin has a structure determined by different deformation phases that have affected the region throughout the Neogene-Quaternary. The accumulation of different orogenic processes, both compressive and extensional, is the cause of the intense brittle deformation of the upper crust and segmentation of the main active faults.

The first processes that determines a heterogeneous behavior in the region are due to the oblique convergence and related compression ( $\sigma_1$ ) between the External and Internal zones during the early Miocene (Figure 8c; Galindo-Zaldívar et al., 1993). These structures only affect the basement, which is only observable in Sierra Elvira, and is characterized by south-vergent thrusting and folds and salt intrusions (Figure 2). However, the boundary between the External and Internal zones is probably more deformed and fractured, which, in the study area, is buried beneath the Granada Basin, near the location of the studied seismicity.

The major structures in the region are more recent. On one hand, the NE-SW faults are extensional and have large associated steps, as it can be seen in the residual gravity map (Figures 4d and 4e). The striae vary between normal and normal to right-lateral, indicating NW-SE or WNW-ESE extension ( $\sigma_3$ ; Figure 8c). Sanz de Galdeano and Vera (1991) consider them to be the result of the gravitational collapse ( $\sigma_1$  vertical) of the late Miocene, which is probably related to the exhumation of the Nevado-Filabride Complex by the Mecina detachment (Jabaloy et al., 1992, 1993).



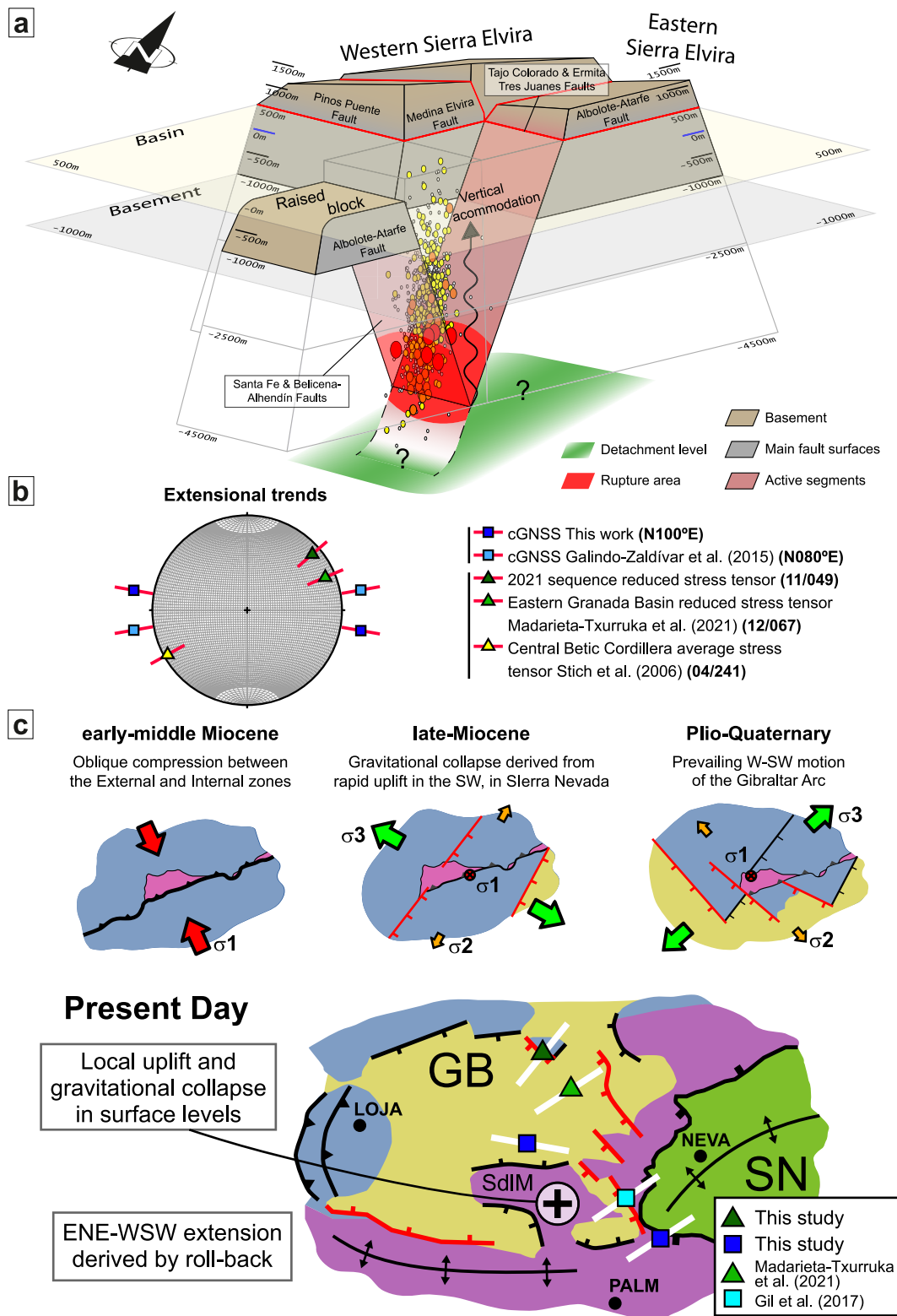


**Figure 8.** Structural model of the Granada Basin seismic area, extensional trends, and evolution. (a) Proposed structural model for the area. (b) Extensional trend obtained by local seismic stress tensors (Madarieta-Txurruka et al., 2021; Stich et al., 2006) and CGPS velocities in the region (Galindo-Zaldívar et al., 2015). (c) Neogene-Quaternary evolution of the Sierra Elvira massif and a new proposal for the present evolution of Sierra Elvira, southern Granada Basin, and Western Sierra Nevada. White lines represent the extension trend in every local area: Triangle:  $\sigma_3$  axis of seismic stress tensors (Madarieta-Txurruka et al., 2021). Squares: CGPS vectors (Gil et al., 2017). GB, Granada Basin. SN, Sierra Nevada. SdlM, Sierra de la Mora.

On the other hand, the most recent and main structures causing seismicity are the NW-SE normal faults. They occur not only in the Santa Fe-Sierra Elvira area, but are also observable throughout the eastern Granada Basin (Madarieta-Txurruka et al., 2021; Sanz de Galdeano et al., 2012). They indicate an NE-SW extension similar to the extension obtained by the reduced stress tensor of the sequence, as well as the stress tensors computed in eastern Granada Basin and central Betic Cordillera (Madarieta-Txurruka et al., 2021; Sparacino et al., 2020; Stich et al., 2006; Figure 8b). They predominate during the Plio-Quaternary and are responsible for the formation of the main depocenters of the Granada Basin (Figure 4d; Rodríguez-Fernández & Sanz de Galdeano, 2006). Together with this set of faults, there are joints with an NE-SW main direction that abound throughout the Sierra Elvira massif (Figures 2 and 3). The Plio-Quaternary activity of these structures could be the result of the permutation of  $\sigma_2$  and  $\sigma_3$ , favored by a low axial stress ratio, the decrease of the gravitational collapse in the SW, and the prevalence of the roll-back that shift toward the W-WSW the Gibraltar Arc (González-Castillo et al., 2015).

### 5.2. Activity of the Seismic Sequence in the Central Granada Basin

The relocation of the seismicity (Figures 5b and 5c) has considerably improved the locations provided by the Spanish IGN (Figure 5a). The new data make it easier to link it to a specific structure and to better understand the causes of seismicity.

The representation of the epicenters of the earthquakes (Figure 5b) indicates that the seismicity is localized in a “spot-shaped” zone no larger than 4 km<sup>2</sup>. We propose, from geological (Figure 2) and gravity data (Figure 4d), that this zone is affected by the two sets of faults described in the previous section. It can be observed that the earthquakes larger than Mw 4.0 are aligned in the NW-SE direction (Figure 5b). In addition, the focal mechanisms reveal the activity of NW-SE faults. Therefore, we consider that most of the earthquakes occur on NW-SE fault planes. In the study area there are NW-SE faults dipping to the SW, see Pinos Puente or Tajo Colorado faults, as well as to the NE, see Santa Fe Fault (Sanz de Galdeano et al., 2010), or the fault bounding the “raised block” to the NE (Figure 4b). The focal mechanisms do not rule out any of the two nodal planes, since they have similar dips. Therefore, either could have been activated. In any case, the seismic sequence does not have an evolution along the fault, as one would expect (Henry & Das, 2001; Scholz, 1990; Stein, 1999; among others) and it is concentrated in a circular zone. This characteristic could be explained by the interaction of the two sets of faults, and the segmentation that occurs between them similar to the barriers defined by Aki (1979). This suggests that the NW-SE set, where the largest earthquakes occur, is segmented by the NE-SW set acting as barriers. This allows stresses not to be transmitted along the fault and to be concentrated in a specific fault segment. We consider this segment to be the equivalent in depth to the 2 km long one of Tajo Colorado Fault, located between the Medina Elvira and Atarfe-Albolote faults (Figures 2, 4d., and 8a). The stresses could be transmitted slightly along the NE-SW faults, upon reaching the intersections between the two sets of faults. In fact, geomorphological and geological data reveal the recent activity of these faults. However, no related focal mechanisms have been observed. This absence could be due to the inactivity of these structures or because they are only capable of generating low-magnitude events. Geologic field data (Figure 2) show a high segmentation of the NE-SW fault set, significantly reducing the occurrence of earthquakes greater than approximately Mw 3.0, from the Wells and Coppersmith (1994) relationships.

Considering the earthquake depth data, the seismic sequence presents a “chimney-shape”. This shape has not been related to any migration over time, therefore it has to be explained spatially. On the one hand, we consider that the largest seismic and deformation zone, between 3 and 5 km, is located just above the detachment of the fault system, related to the one proposed by Madarieta-Txurruka et al. (2021). The detachment would separate a footwall block from a highly brittle deformed hanging wall block. On the other hand, unlike traditional models, the intersection of fault sets acts as a barrier. Because of this, the deformation is not transmitted along the fault, but vertically. The great fragmentation of the region, both by faults and vertical joints (Figures 2 and 3), could facilitate the upwards migration of deformation.

### 5.3. Inferences for the Seismic Potential in the Area Affected by the Granada 2021 Sequence

The accurate relocation of seismicity provides information to define Subsurface Rupture Length (SbRL) and RA. These are then used to estimate the expected magnitude ( $M_{\text{segment}}$ ) for an earthquake occurring in the proposed segment, and the expected seismic moment ( $M_0$ ) for the rupture of the seismogenic segment. An SbRL value



equal to 2 km has been selected, equivalent to the segment located between the Medina Elvira and Atarfe-Albolote faults. An RA value equal to approximately 5.6 km<sup>2</sup> is estimated considering that most of the earthquakes occur between 3 and 5 km and faults dip 45° (obtained from focal mechanisms solutions). In this way, the computed  $M_{\text{segment}}$  value from RA is Mw 4.7–4.7, and from SbRL, Mw 4.6–4.8, depending on the used scaling equation (Leonard, 2010; Wells & Coppersmith, 1994). The computed  $M_0$  value is  $1.7 \times 10^{16}$  N-m, calculated from RA, and  $1.0 \times 10^{16}$  N-m, calculated from SbRL. These values make it possible to compare the proposed model with the data and discuss the seismic potential associated to this phenomenon.  $M_{\text{segment}}$  values of Mw 4.7–4.8 are slightly higher than the largest earthquakes of the 2021 sequence, and of the order of the equivalent magnitude of the first phase ( $\sim m_{\text{bLg}}$  4.8). They indicate that the segment at depth could be a little smaller than the one observed at surface, or that a part of the segment has remained unbroken. Previous  $M_0$  values, obtained for the proposed model, are less than what calculated for the first phase from the recorded magnitudes of  $2.25 \times 10^{16}$  N-m. These data support the importance of barriers to localizing the seismicity in the restricted segment and above it. Moreover, it explains the swarm-like behavior of the beginning of the phase instead of one major earthquake. Several events did not exceed the proposed magnitude of the rupture area, resulting in a reduction of the seismic potential in this highly segmented sector with respect to other areas of the region.

The propagation of seismic waves and the phenomena related to low deformations in soils are influenced, among others, by lithological characteristics of the surface rocks (NCSE-02, 2002). Earthquakes of these expected magnitudes will affect the zones of Sierra Elvira, and the zones located on the deposits of the Granada Basin, in different ways. This is because rock type soils formed by limestones, dolomites and silex fragments are found in Sierra Elvira (Figure 2; Lupiani & Soria, 1988). The elastic-brittle character of these soils prevent amplification of seismic waves. However, the sediments of the basin, in the Atarfe sector, are formed by soils geotechnically classified as transitional; specifically marl limestones and marls together with alluvial soils. Given the cohesive nature of these soils, the presence of shallow water tables (according to soundings averaging 5 m) and their open and impermeable structure (CEGP, 2012; Suarez, 2021), will produce a certain ground motion amplification, increasing building damages. The elasto-plastic ductile deformability and impermeable character of the cohesive soils will produce the accumulation of deformations in each event and more long-term pathologies (NCSE-02, 2002).

#### 5.4. The Active Deformation of the South-Central Betic Cordillera: Seismic Stress Tensor and CGPS Data Discrepancy

The velocity vectors obtained from the CGPS indicate a westward displacement of the sites (Figures 7, 8b, and 8c), however, this does not occur in the same way. Considering NEVA as fixed, PALM shifts to the SW, in a similar direction with respect to the rest of the extension indicators (Figures 1–3, 6d, and 7; Madarieta-Txurruka et al., 2021; Stich et al., 2006). However, LOJA shifts to the W-NW, similarly to the values published by Galindo-Zaldívar et al. (2015) between stations GRA1 and LOJA (Figures 1 and 8b). This indicates a westward displacement of the hanging wall block of the Mecina detachment (Galindo-Zaldívar et al., 1996; Madarieta-Txurruka et al., 2021) related to slab-tearing processes (Booth-Rea et al., 2012, 2007; Mancilla et al., 2015) or roll-back and the westward migration of the Gibraltar Arc (Galindo-Zaldívar et al., 2015; Garate et al., 2015; González-Castillo et al., 2015; Koulali et al., 2011). Meanwhile, a clockwise rotation of  $\sigma_3$  in LOJA with respect to PALM, and the stress determined from earthquake focal mechanisms could be related to an N-S heterogeneous extension related to the uplift of the central Betic Cordillera and related gravitational collapse affecting the southern Granada Basin, also evidenced by the local elevation near Sierra de la Mora (Figure 8c).

#### 5.5. Implications for the Study of Tectonic Seismic Sequences

The second and shorter phase (in August 2021) is clearly a mainshock-aftershock sequence. The first and most important phase has characteristics of both types, mainshock-aftershock and seismic swarm, suggesting that a more detailed study is necessary. Therefore, we will adopt the parameters proposed by Vidale et al. (2006) and Vidale and Shearer (2006): (a) cloud size with respect to the cumulative seismic moment, (b) number of aftershocks, (c) time of the largest event, and (d) expansion of the seismicity zone. On one hand, the data indicate a small size of the earthquake cloud for the computed cumulative seismic moment, common in mainshock-aftershock sequences. However, the number of aftershocks is high with respect to the largest event, an Mw 4.5 earthquake, pointing to a swarm (Vidale et al., 2006). The first earthquake in the phase is not the high-

est, but this occurs early in the sequence, 3 days later in a sequence that lasts for 4 months. In fact, if we consider the cumulative seismic moment decay and  $b$ -value, equal to 0.93, this also points to a mainshock-aftershock sequence (Frohlich & Davis, 1993). Finally, the hypocenter cloud does not show any expansion. In addition, geometrically, the Granada seismic sequence has a very low planarity (0.1) for sub-vertical sequences related to normal faults, if we compare it with studies of seismic sequences from California (Vidale & Shearer, 2006), Japan (Vidale et al., 2006) and other parts of the Betic Cordillera (Carmona et al., 2009; Hamdache et al., 2019; Morales et al., 2015; Ocaña, 2009). All of these features require a new explanation for the causes of this sequence.

Usually, the sequences with limited extensions in the horizontal and vertical axes, that is, “chimneys-shaped”, are related to volcanic zones. However, we do not find ourselves in that context. Therefore, we believe that barriers and inherited brittle deformation play a very important role in this case, helped by fluids. We propose a model where the seismicity occurs due to the accumulation of stresses in the area, and it is triggered by fluids in the detachment zone (Sibson, 2000). In fact, fluids are common in the region (Figure 3j; e.g., García-Veigas et al., 2015; Kohfahl et al., 2008). In this scenario, the perpendicular fault set acts as a barrier. On one hand, it does not allow the occurrence of earthquakes larger than expected for the segment and, on the other hand, they prevent the expansion and migration along the fault of the sequence. Instead, the deformation is transmitted vertically to the surface, facilitated by fractures, especially vertical tensional joints (Figure 3), and probably by fluid uplift (Figure 3j; Sibson, 2000). Thus, the first phase has a “swarmy” behavior at the beginning, several earthquakes of similar magnitude occur without one of them standing out. Then, aftershocks follow in a cascade model triggered by each largest earthquake (Henry & Das, 2001; Stein, 1999; Scholz, 1990; among others).

## 6. Conclusions

The integration of seismology, geological, geophysical prospecting, and geodetical studies made it possible to establish the structure of the Granada Basin, as well as to identify the seismogenic structures responsible for the Granada 2021 seismic sequence and to frame it in the evolution of the central Betic Cordillera.

The highly intense and variable recent geodynamic processes of the central Betic Cordillera have been responsible, since the early Miocene, for the high brittle deformation of the area affected by the 2021 seismic sequence in Granada. This recent evolution produced a basement affected by two main sets of faults, striking NE-SW and NW-SE. Both sets of faults are responsible for the uplift of the Sierra Elvira horst, and another raised block to the SW buried below the sedimentary infill. At the same time, they generated the main depocenters of the eastern Granada Basin.

The 2021 seismicity has a “chimney-shaped” morphology. The lineation of the main earthquakes suggests the activity of NW-SE faults. However, the seismicity is very localized and it is associated with the activity of a specific segment about 2 km long. The cumulative moment tensor calculated for the sequence, equivalent to an Mw 4.8 earthquake, matches the proposed segment rupture length. The NE-SW fault set acts as a barrier and is responsible for the segmentation of the main fault set. This segmentation confines the seismicity and does not allow the migration along the fault. Vertically, the sequence has a tubular shape in which the largest earthquakes are concentrated above 5 km depth, over the detachment zone of the Granada extensional system. The deformation in this zone, unable to be transmitted along the fault, migrates upwards facilitated by the preexisting fractures and probably helped by fluid uplift.

There is a striking discrepancy between the extension vectors calculated from the stress tensors of focal mechanisms (<15 km) and the surface CGPS data. It could be due to a heterogeneous local uplift that raised basement blocks in the S of the basin, generating gravity collapse processes and the rotation of the  $\sigma_3$  axis at the surface.

The relationship between subsurface rupture length and RA with  $M_{\text{segment}}$  and  $M_0$  suggests the occurrence of earthquakes with magnitudes up to Mw 4.6–4.8, slightly higher than the main earthquakes of the sequence. That comparison demonstrates that the main earthquakes of the sequence fit with the proposed segment. In the same way, this relationship suggests that barriers do not allow larger earthquakes to occur and stresses are released by several events equivalent to the proposed segment, giving the sequence “swarmy” features at the beginning.

The example of the Granada seismic sequence highlights the importance of the interaction between oblique fault sets in fault segmentation and in acting as barrier to confine seismic sequences and propagating the deformation



unconventionally. Moreover, it provides a new explanation for seismic sequence with both mainshock-aftershock and swarm characteristics.

## Data Availability Statement

The authors also thank the IGN for sharing seismicity data, focal mechanisms and DTMs through their online databases at <http://www.ign.es/web/ign/portal/sis-catalogo-terremotos>, <https://www.ign.es/web/ign/portal/tensor-momento-sismico/>, and <http://centrodedescargas.cnig.es/CentroDescargas/> respectively. The authors also thank the Instituto Geológico y Minero de España (IGME-CSIC) for sharing the Bouguer anomaly data from the website <http://info.igme.es/SIGEOF/> and active fault data from the Quaternary Faults Database of Iberia at <https://info.igme.es/qaf/>.

## Acknowledgments

The authors would like to thank the two anonymous reviewers for their constructive comments that improved the quality of this article and Dr. Taylor Schildgen and Dr. Luca Dal Zilio for their editorial handling of the manuscript. This study was supported by the Spanish projects Evaluación de la Peligrosidad de Inestabilidades de Laderas Asociadas a Terremotos (CGL2015-65602-R AEI-FEDER); P18-RT-3275 and B-RNM-301-UGR18 (Junta de Andalucía/FEDER); Programa Operativo FEDER Andalucía 2014–2020 – call made by the University of Jaén (Ref. 126344); POAIUJA 2021/2022 from the University of Jaén, as well as the Andalusian research groups RNM-148, RNM-282, and RNM-370. Funding for open access charge: Universidad de Granada/CBU.

## References

- Aki, K. (1979). Characterization of barriers on an earthquake fault. *Journal of Geophysical Research*, 84(B11), 6140–6148. <https://doi.org/10.1029/JB084iB11p06140>
- Aldaya, F., Alvarez, F., Galindo-Zaldívar, J., González-Lodeiro, F., & Jabaloy, A. (1991). The Maláguide-Alpujarride contact (Betic Cordilleras, Spain): A brittle extensional detachment. *Comptes Rendus de l'Académie Des Sciences. Série II, Mécanique, Physique, Chimie, Sciences de l'univers, Sciences de La Terre*, 313(12), 1447–1453.
- Andrieux, J., Fontbote, J. M., & Mattauer, M. (1971). Sur un modele explicatif de l'arc de Gibraltar. *Earth and Planetary Science Letters*, 12(2), 191–198. [https://doi.org/10.1016/0012-821X\(71\)90077-X](https://doi.org/10.1016/0012-821X(71)90077-X)
- Araña, V., & Vegas, R. (1974). Plate tectonics and volcanism in the Gibraltar Arc. *Tectonophysics*, 24(3), 197–212. [https://doi.org/10.1016/0040-1951\(74\)90008-0](https://doi.org/10.1016/0040-1951(74)90008-0)
- Ayala, C., Bohoyo, F., Maestro, A., Reguera, M. I., Torne, M., Rubio, F., et al. (2016). Updated Bouguer anomalies of the Iberian Peninsula: A new perspective to interpret the regional geology. *Journal of Maps*, 12(5), 1089–1092. <https://doi.org/10.1080/17445647.2015.1126538>
- Banks, C. J., & Warburton, J. (1991). Mid-crustal detachment in the Betic system of southeast Spain. *Tectonophysics*, 191(3–4), 275–289. [https://doi.org/10.1016/0040-1951\(91\)90062-W](https://doi.org/10.1016/0040-1951(91)90062-W)
- Benoit, J. P., & McNutt, S. R. (1996). Global volcanic earthquake swarm database and preliminary analysis of volcanic earthquake swarm duration. *Annali di Geofisica*, 39(2), 221. <https://doi.org/10.4401/ag-3963>
- Bertiger, W., Bar-Sever, Y., Dorsey, A., Haines, B., Harvey, N., & Hemberger, D. (2020). GipsyX/RTGx, a new tool set for space geodetic operations and research. *Advances in Space Research*, 66(3), 469–489. <https://doi.org/10.1016/j.asr.2020.04.015>
- Bird, P. (2003). An updated digital model of plate boundaries. *Geochemistry, Geophysics, Geosystems*, 4(3), 1027. <https://doi.org/10.1029/2001GC000252>
- Blakely, R. (1996). *Potential theory in gravity and magnetic applications*. Cambridge, U.K. Cambridge University Press.
- Blanco, M. J., & Spakman, W. (1993). The P wave velocity structure of the mantle below the Iberian Peninsula: Evidence for subducted lithosphere below southern Spain. *Tectonophysics*, 221(1), 13–34. [https://doi.org/10.1016/0040-1951\(93\)90025-F](https://doi.org/10.1016/0040-1951(93)90025-F)
- Booth-Rea, G., Jabaloy-Sánchez, A., Azdimousa, A., Asebriy, L., Vilchez, M. V., & Martínez-Martínez, J. M. (2012). Upper-crustal extension during oblique collision: The Tensamane extensional detachment (eastern Rif, Morocco). *Terra Nova*, 24(6), 505–512. <https://doi.org/10.1111/j.1365-3121.2012.01089.x>
- Booth-Rea, G., Ranero, C., Grevemeyer, I., & Martínez-Martínez, J. (2007). Crustal types and tertiary tectonic evolution of the Alborán Sea, western Mediterranean. *Geochemistry, Geophysics, Geosystems*, 8(10), Q10005. <https://doi.org/10.1029/2007GC001639>
- Braga, J. C., Jiménez, A., & Rivas, P. (1979). El Jurásico de Sierra Elvira (estudio especial del Lías medio y superior). *Cuad. Geol. Univ. Granada*, 10, 597–604.
- Braga, J. C., Martín, J., & Quesada, C. (2003). Patterns and average rates of late Neogene-recent uplift of the Betic Cordillera, SE Spain. *Geomorphology*, 50(1–3), 3–26. [https://doi.org/10.1016/S0169-555X\(02\)00205-2](https://doi.org/10.1016/S0169-555X(02)00205-2)
- Braga, J. C., Martín, J. M., & Alcalá, B. (1990). Coral reefs in coarse-terrigenous sedimentary environments (Upper Tortonian, Granada Basin, southern Spain). *Sedimentary Geology*, 66(1–2), 135–150. [https://doi.org/10.1016/0037-0738\(90\)90011-H](https://doi.org/10.1016/0037-0738(90)90011-H)
- Bufo, E., Cesca, S., Góded, T., Fresno, C. D., & Muñoz, D. (2006). The Bullas (Murcia, SE Spain) earthquake, 29 January 2005. *Journal of Seismology*, 10(1), 65–72. <https://doi.org/10.1007/s10950-006-2536-9>
- Bufo, E., Pro, C., Cesca, S., Udías, A., & del Fresno, C. (2011). The 2010 Granada, Spain, deep earthquake. *Bulletin of the Seismological Society of America*, 101(5), 2418–2430. <https://doi.org/10.1785/0120110022>
- Calvert, A., Sandvol, E., Seber, D., Barazangi, M., Vidal, F., Alguacil, G., & Jabour, N. (2000). Propagation of regional seismic phases (Lg and Sn) and Pn velocity structure along the Africa-Iberia plate boundary zone: Tectonic implications. *Geophysical Journal International*, 142(2), 384–408. <https://doi.org/10.1046/j.1365-246X.2000.00160.x>
- Carminati, E., Lustrino, M., & Doglioni, C. (2012). Geodynamic evolution of the central and western Mediterranean: Tectonics vs. igneous petrology constraints. *Tectonophysics*, 579, 173–192. <https://doi.org/10.1016/j.tecto.2012.01.026>
- Carmona, E., Stich, D., Ibañez, J. M., & Saccorotti, G. (2009). Multiplet focal mechanisms from polarities and relative locations: The Iznajar swarm in southern Spain. *Bulletin of the Seismological Society of America*, 99(6), 3421–3429. <https://doi.org/10.1785/0120090036>
- Cattania, C., Hainzl, S., Wang, L., Enescu, B., & Roth, F. (2015). Aftershock triggering by postseismic stresses: A study based on Coulomb rate-and-state models. *Journal of Geophysical Research: Solid Earth*, 120(4), 2388–2407. <https://doi.org/10.1002/2014JB011500>
- CEGP (2012). Análisis de Riesgo Aplicado a la Seguridad en Presas y Embalses, P-8 Comité Español de Grandes Presas.
- Chertova, M., Spakman, W., Geenen, T., van den Berg, A., & van Hinsbergen, D. (2014). Underpinning tectonic reconstructions of the western Mediterranean region with dynamic slab evolution from 3-D numerical modeling. *Journal of Geophysical Research: Solid Earth*, 119, 3678–3902. <https://doi.org/10.1002/2014JB011150>
- Chlieh, M., Avouac, J. P., Sieh, K., Natawidjaja, D. H., & Galetzka, J. (2008). Heterogeneous coupling of the Sumatran megathrust constrained by geodetic and paleogeodetic measurements. *Journal of Geophysical Research: Solid Earth*, 113(B5). <https://doi.org/10.1029/2007JB004981>
- CNIG. (2022). Download center of National Center of Geographic Information (CNIG). IGN. Retrieved from <http://centrodedescargas.cnig.es/CentroDescargas/index.jsp>

- Comas, M. C., Platt, J. P., Soto, J. I., & Watts, A. B. (1999). The origin and tectonic history of the Alboran Basin: Insights from leg 161 results. *Proceedings of the Ocean Drilling Program Scientific Results*, 161, 555–580.
- Crespo-Blanc, A. (1995). Interference pattern of extensional fault systems: A case study of the Miocene rifting of the Alboran basement (North of Sierra Nevada, Betic Chain). *Journal of Structural Geology*, 17(11), 1559–1569. [https://doi.org/10.1016/0191-8141\(95\)E0044-D](https://doi.org/10.1016/0191-8141(95)E0044-D)
- D'Acremont, E., Gutscher, M., Rabaute, A., Mercier de Lépinay, B., Lafosse, M., Poort, J., et al. (2014). High-resolution imagery of active faulting offshore Al Hoceima, Northern Morocco. *Tectonophysics*, 632(C), 160–166. <https://doi.org/10.1016/j.tecto.2014.06.008>
- de Vicente, G., Cloetingh, S., Muñoz-Martín, A., Olaiz, A., Stich, D., Vegas, R., et al. (2008). Inversion of moment tensor focal mechanisms for active stresses around the microcontinent Iberia: Tectonic implications. *Tectonics*, 27(1), 1. <https://doi.org/10.1029/2006TC002093>
- Delvaux, D., & Barth, A. (2010). African stress pattern from formal inversion of focal mechanism data. *Tectonophysics*, 482(1–4), 105–128. <https://doi.org/10.1016/j.tecto.2009.05.009>
- Delvaux, D., & Sperner, B. (2003). New aspects of tectonic stress inversion with reference to the TENSOR program. *Geological Society Special Publication*, 212, 75–100. <https://doi.org/10.1144/GSL.SP.2003.212.01.06>
- DeMets, C., Gordon, R. G., & Argus, D. F. (2010). Geologically current plate motions. *Geophysical Journal International*, 181(1), 1–80. <https://doi.org/10.1111/j.1365-246X.2009.04491.x>
- Dixon, T. H. (1991). An introduction to the Global Positioning System and some geological applications. *Reviews of Geophysics*, 29(2), 249–276. <https://doi.org/10.1029/91RG00152>
- Duggen, S., Hoernie, K., Van den Bogaard, P., Rüpke, L., & Morgan, J. P. (2003). Deep roots of the Messinian salinity crisis. *Nature*, 422(6932), 602–606. <https://doi.org/10.1038/nature01553>
- Durand-Delga, M., Rossi, P., Olivier, P., & Puglisi, D. (2000). Situation structurale et nature ophiolitique de roches basiques jurassiques associées aux flyschs maghrébins du Rif (Maroc) et de Sicile (Italie). *Comptes Rendus de l'Académie des Sciences—Serie IIa: Sciences de La Terre et Des Planetes*, 331(1), 29–38. [https://doi.org/10.1016/S1251-8050\(00\)01378-1](https://doi.org/10.1016/S1251-8050(00)01378-1)
- DuRoss, C. B., & Hylland, M. D. (2015). Synchronous ruptures along a major graben-forming fault system: Wasatch and West Valley Fault Zones, Utah. *Bulletin of the Seismological Society of America*, 105(1), 14–37. <https://doi.org/10.1785/0120140064>
- Dziak, R. P., Chadwick, W. W., Jr., Fox, C. G., & Embley, R. W. (2003). Hydrothermal temperature changes at the southern Juan de Fuca Ridge associated with Mw 6.2 Blanco Transform earthquake. *Geology*, 31(2), 119–122. [https://doi.org/10.1130/0091-7613\(2003\)031<0119:htcats>2.0.co;2](https://doi.org/10.1130/0091-7613(2003)031<0119:htcats>2.0.co;2)
- Endo, E. T., Malone, S. D., Nosen, L. L., & Weaver, C. S. (1981). Locations, magnitudes, and statistics of the 20 March to 18 May earthquake sequence. In P. W. Lipman, & D. R. Mullineaux (Eds.), *The 1980 eruptions of Mount St. Helens* (pp. 93–107). Washington, DC: Geological.
- Faccenna, C., Piromallo, C., Crespo-Blanc, A., Jolivet, L., & Rossetti, F. (2004). Lateral slab deformation and the origin of the western Mediterranean arcs. *Tectonics*, 23, TC1012. <https://doi.org/10.1029/2002TC001488>
- Fallot, P. (1948). Les cordillères bétiques. *Estudios Geológicos*, 4, 259–279.
- Fernández-Fernández, E. M., Jabaloy-Sánchez, A., Nieto, F., & González-Lodeiro, F. (2007). Structure of the Maláguide complex near Vélez Rubio (Eastern Betic Cordillera, SE Spain). *Tectonics*, 26(4), TC4008. <https://doi.org/10.1029/2006TC002019>
- Fontboté, J. M., & Estévez, A. (1980). Geología de las Cordilleras Béticas. *Boletín Geológico y Minero*, 91–92.
- Freed, A. M. (2005). Earthquake triggering by static, dynamic, and postseismic stress transfer. *Annual Review of Earth and Planetary Sciences*, 33(1), 335–367. <https://doi.org/10.1146/annurev.earth.33.092203.122505>
- Frohlich, C., & Davis, S. D. (1993). Teleseismic *b* values; or, Much Ado about 1.0. *Journal of Geophysical Research*, 98(B1), 631–644. <https://doi.org/10.1029/92JB01891>
- Fullea, J., Fernández, M., & Zeyen, H. (2008). FA2BOUG-A FORTRAN 90 code to compute Bouguer gravity anomalies from gridded free-air anomalies: Application to the Atlantic-Mediterranean transition zone. *Computers & Geosciences*, 34(12), 1665–1681. <https://doi.org/10.1016/j.cageo.2008.02.018>
- Galindo-Zaldívar, J., Ercilla, G., Estrada, F., Catalán, M., d'Acremont, E., & Azzouz, O. (2018). Imaging the growth of recent faults: The case of 2016–2017 seismic sequence sea bottom deformation in the Alboran Sea (western Mediterranean). *Tectonics*, 37(8), 2513–2530. <https://doi.org/10.1029/2017TC004941>
- Galindo-Zaldívar, J., Gil, A., Borque, M., González-Lodeiro, F., Jabaloy, A., Marín-Lechado, C., et al. (2003). Active faulting in the internal zones of the central Betic Cordilleras (SE, Spain). *Journal of Geodynamics*, 36(1–2), 239–250. [https://doi.org/10.1016/S0264-3707\(03\)00049-8](https://doi.org/10.1016/S0264-3707(03)00049-8)
- Galindo-Zaldívar, J., Gil, A., Sanz de Galdeano, C., Lacy, M., García-Armenteros, J., Ruano, P., et al. (2015). Active shallow extension in central and eastern Betic Cordillera from CGPS data. *Tectonophysics*, 663, 290–301. <https://doi.org/10.1016/j.tecto.2015.08.035>
- Galindo-Zaldívar, J., Gonzalez-Lodeiro, F., & Jabaloy, A. (1989). Structures progressives en cisaillement extensif dans un détachement à la partie occidentale de la Sierra Nevada (Cordillères bétiques, Espagne). *Geodinamica Acta*, 3(1), 73–85. <https://doi.org/10.1080/09853111.1989.1105175>
- Galindo-Zaldívar, J., González-Lodeiro, F., & Jabaloy, A. (1991). Geometry and kinematics of post-Aquitania brittle deformation in the Alpujarride rocks and their relation with the Alpujarride/Nevado-Filábride contact. *Geogaceta*, 10, 130–134. <http://hdl.handle.net/10272/18063>
- Galindo-Zaldívar, J., González-Lodeiro, F., & Jabaloy, A. (1993). Stress and paleostress in the Betic-Rif cordilleras (Miocene to the present). *Tectonophysics*, 227(1–4), 105–126. [https://doi.org/10.1016/0040-1951\(93\)90090-7](https://doi.org/10.1016/0040-1951(93)90090-7)
- Galindo-Zaldívar, J., Jabaloy, A., & Gonzalez-Lodeiro, F. (1996). Reactivation du détachement extensif de Mecina dans le secteur occidental de la Sierra Nevada (Cordillères bétiques, SE de l'Espagne). *Comptes Rendus de l'Académie des Sciences-Serie IIa-Sciences de La Terre et Des Planetes*, 323(7), 615–622.
- Galindo-Zaldívar, J., Jabaloy, A., Serrano, I., Morales, J., González-Lodeiro, F., & Torcal, F. (1999). Recent and present-day stresses in the Granada Basin (Betic Cordilleras): Example of a late Miocene-present-day extensional basin in a convergent plate boundary. *Tectonics*, 18(4), 686–702. <https://doi.org/10.1029/1999TC900016>
- Garate, J., Martin-Davila, J., Khazaradze, G., Echeverria, A., Asensio, E., Gil, A. J., et al. (2015). Topo-Iberia project: CGPS crustal velocity field in the Iberian Peninsula and Morocco. *GPS Solutions*, 19(2), 287–295. <https://doi.org/10.1007/s10291-014-0387-3>
- García-Alix, A., Minwer-Barakat, R., Martín, J. M., Suárez, E. M., & Freudenthal, M. (2008). Biostratigraphy and sedimentary evolution of late Miocene and Pliocene continental deposits of the Granada Basin (southern Spain). *Lethaia*, 41(4), 431–446. <https://doi.org/10.1111/j.1502-3931.2008.00097.x>
- García-Alix, A., Minwer-Barakat, R., Martín, J. M., Suárez, E. M., & Freudenthal, M. (2009). Dating the change from endorheic to exorheic conditions in the drainage system of the Granada Basin (Southern Spain). *Palaios*, 24(8), 544–549. <https://doi.org/10.2110/palo.2009.p09-015r>
- García-Dueñas, V. (1967). *Geología de la Zona Subbética al Norte de Granada*, (Doctoral dissertation). Universidad de Granada.
- García-Dueñas, V., Balanyá, J., & Martínez-Martínez, J. (1992). Miocene extensional detachments in the outcropping basement of the northern Alboran Basin (Betics) and their tectonic implications. *Geo-Marine Letters*, 12(2–3), 88–95. <https://doi.org/10.1007/BF02084917>



- García-Hernández, M., López-Garrido, A. C., Rivas, P., Sanz de Galdeano, C., & Vera, J. A. (1980). Mesozoic paleogeographic evolution of the external zones of the Betic Cordillera. *Geologie en Mijnbouw*, 59(2), 155–168. <http://hdl.handle.net/10261/29167>
- García-Mayordomo, J., & Martín-Banda, R. (2022). Guide for the use of QAFI v.4. In: <http://info.igme.es/qafi/>—Instituto Geológico y Minero de España (IGME), CSIC, Madrid, Spain. <https://doi.org/10.13140/RG.2.2.12873.01121>
- García-Veigas, J., Rosell, L., Cendón, D. I., Gibert, L., Martín, J. M., Torres-Ruiz, J., & Orti, F. (2015). Large celestine orebodies formed by early-diagenetic replacement of gypsified stromatolites (Upper Miocene, Monteveve-Escúzar deposit, Granada Basin, Spain). *Ore Geology Reviews*, 64, 187–199. <https://doi.org/10.1016/j.oregeorev.2014.07.009>
- Gil, A. J., Galindo-Zaldívar, J., de Galdeano, C. S., Borque, M. J., Sánchez-Alzola, A., Martínez-Martos, M., & Alfaro, P. (2017). The Padul normal fault activity constrained by GPS data: Brittle extension orthogonal to folding in the central Betic Cordillera. *Tectonophysics*, 712, 64–71. <https://doi.org/10.1016/j.tecto.2017.05.008>
- Gomberg, J., & Johnson, P. (2005). Dynamic triggering of earthquakes. *Nature*, 437(7060), 830. <https://doi.org/10.1038/437830a>
- Gómez-Pugnaire, M. T., Rubatto, D., Fernández-Soler, J. M., Jabaloy, A., López Sánchez-Vizcaíno, V., González-Lodeiro, F., et al. (2012). Late Variscan magmatism in the Nevado-Filábride complex: U-Pb geochronologic evidence for the pre-Mesozoic nature of the deepest Betic complex (SE Spain). *Lithos*, 146–147, 93–111. <https://doi.org/10.1016/j.lithos.2012.03.027>
- González-Castillo, L., Galindo-Zaldívar, J., de Lacy, M. C., Borque, M. J., Martínez-Moreno, F. J., García-Armenteros, J. A., & Gil, A. J. (2015). Active rollback in the Gibraltar Arc: Evidences from CGPS data in the western Betic Cordillera. *Tectonophysics*, 663, 310–321. <https://doi.org/10.1016/j.tecto.2015.03.010>
- Grauch, V. J. S., & Cordell, L. (1987). Short note: Limitations of determining density or magnetic boundaries from horizontal gradient of gravity or pseudogravity data. *Geophysics*, 52(1), 118–121. <https://doi.org/10.1190/1.1442236>
- Grünthal, G. (1998). European macroseismic scale 1998. *Cahiers du Centre Européen de Géodynamique et de Séismologie* (Vol. 15).
- Gupta, A., & Scholz, C. H. (2000). A model of normal fault interaction based on observations and theory. *Journal of Structural Geology*, 22(7), 865–879. [https://doi.org/10.1016/S0191-8141\(00\)00011-0](https://doi.org/10.1016/S0191-8141(00)00011-0)
- Gutenberg, B., & Richter, C. (1944). Frequency of earthquakes in California. *Bulletin of the Seismological Society of America*, 34(4), 185–188. <https://doi.org/10.1785/BSSA0340040185>
- Gutscher, M. A. (2004). What caused the great Lisbon earthquake? *Science*, 305(5688), 1247–1248. <https://doi.org/10.1126/science.1101351>
- Hager, B. H., King, R. W., & Murray, M. H. (1991). Measurement of crustal deformation using the Global Positioning System. *Annual Review of Earth and Planetary Sciences*, 19(1), 351–382. <https://doi.org/10.1146/annurev.earth.19.050191.002031>
- Hainzl, S. (2004). Seismicity patterns of earthquake swarms due to fluid intrusion and stress triggering. *Geophysical Journal International*, 159(3), 1090–1096. <https://doi.org/10.1111/j.1365-246X.2004.02463.x>
- Hainzl, S., & Fischer, T. (2002). Indications for a successively triggered rupture growth underlying the 2000 earthquake swarm in Vogtland/NW Bohemia. *Journal of Geophysical Research: Solid Earth*, 107(B12), ESE5-1–ESE5-9. <https://doi.org/10.1029/2002JB001865>
- Hamdache, M., Henares, J., Peláez, J. A., & Damerджи, Y. (2019). Fractal analysis of earthquake sequences in the Ibero-Maghreb region. *Pure and Applied Geophysics*, 176(4), 1397–1416. <https://doi.org/10.1007/s00024-018-2072-x>
- Hamdache, M., Peláez, J. A., Henares, J., Damerджи, Y., & Sawires, R. (2016). Analysis of the 2012–2013 Torroperogil-Sabiote seismic swarm. *Physics and Chemistry of the Earth*, 95, 101–112. <https://doi.org/10.1016/j.pce.2016.01.003>
- Hanks, T. C., & Kanamori, H. (1979). A moment magnitude scale. *Journal of Geophysical Research: Solid Earth*, 84(B5), 2348–2350. <https://doi.org/10.1029/JB084iB05p02348>
- Harris, R. A. (1998). Introduction to special section: Stress triggers, stress shadows, and implications for seismic hazard. *Journal of Geophysical Research: Solid Earth*, 103(B10), 24347–24358. <https://doi.org/10.1029/98JB01576>
- Harris, R. A. (2004). Numerical simulations of large earthquakes: Dynamic rupture propagation on heterogeneous faults. In A. Donnellan, P. Mora, M. Matsu'ura, & X. C. Yin (Eds.), *Computational earthquake science part II. PAGEOPH topical volumes* (pp. 2171–2181). Birkhäuser, Basel. [https://doi.org/10.1007/978-3-0348-7875-3\\_5](https://doi.org/10.1007/978-3-0348-7875-3_5)
- Hatch, R. L., Abercrombie, R. E., Ruhl, C. J., & Smith, K. D. (2020). Evidence of aseismic and fluid-driven processes in a small complex seismic swarm near Virginia City, Nevada. *Geophysical Research Letters*, 47(4), e2019GL085477. <https://doi.org/10.1029/2019GL085477>
- Hayashi, Y., & Morita, Y. (2003). An image of a magma intrusion process inferred from precise hypocentral migrations of the earthquake swarm east of the Izu Peninsula. *Geophysical Journal International*, 153(1), 159–174. <https://doi.org/10.1046/j.1365-246X.2003.01892.x>
- Henry, C., & Das, S. (2001). Aftershock zones of large shallow earthquakes: Fault dimensions, aftershock area expansion, and scaling relations. *Geophysical Journal International*, 147(2), 272–293. <https://doi.org/10.1046/j.1365-246X.2001.00522.x>
- Hill, D. P. (1977). A model for earthquake swarms. *Journal of Geophysical Research*, 82(8), 1347–1352. <https://doi.org/10.1029/JB082i008p01347>
- Hill, D. P., & Prejean, S. G. (2015). Dynamic triggering. In G. Schubert (Ed.), *Treatise on geophysics* (pp. 273–304). Elsevier. <https://doi.org/10.1016/b978-0-444-53802-4.00078-6>
- Hurst, A. W., & McGinty, P. J. (1999). Earthquake swarms to the west of Mt Ruapehu preceding its 1995 eruption. *Journal of Volcanology and Geothermal Research*, 90(1–2), 19–28. [https://doi.org/10.1016/S0377-0273\(99\)00019-0](https://doi.org/10.1016/S0377-0273(99)00019-0)
- Ibs-von Seht, M., Plenefisch, T., & Klinge, K. (2008). Earthquake swarms in continental rifts—A comparison of selected cases in America, Africa, and Europe. *Tectonophysics*, 452(1–4), 66–77. <https://doi.org/10.1016/j.tecto.2008.02.008>
- Informe, I. G. N. (2021). Informe de la actividad sísmica en Atarde-Santa Fe (Granada). Retrieved from [https://www.ign.es/resources/sismologia/noticias/InformeIGN\\_SantaFe.pdf](https://www.ign.es/resources/sismologia/noticias/InformeIGN_SantaFe.pdf)
- Iribarren, L., Vergés, J., Camurri, F., Fullea, J., & Fernández, M. (2007). The structure of the Atlantic-Mediterranean transition zone from the Alboran Sea to the Horseshoe Abyssal Plain (Iberia-Africa plate boundary). *Marine Geology*, 243(1–4), 97–119. <https://doi.org/10.1016/j.margeo.2007.05.011>
- Jabaloy, A., Galindo-Zaldívar, J., & González-Lodeiro, F. (1992). The Mecina extensional system: Its relation with the post-Aquitania piggy-back basins and the paleostresses evolution (Betic Cordilleras, Spain). *Geo-Marine Letters*, 12(2–3), 96–103. <https://doi.org/10.1007/BF02084918>
- Jabaloy, A., Galindo-Zaldívar, J., & González-Lodeiro, F. (1993). The Alpujárride-Nevado-Filábride extensional shear zone, Betic Cordillera, SE Spain. *Journal of Structural Geology*, 15(3–5), 555–569. [https://doi.org/10.1016/0191-8141\(93\)90148-4](https://doi.org/10.1016/0191-8141(93)90148-4)
- Kane, M. (1962). A comprehensive system of terrain corrections using a digital computer. *Geophysics*, 27(4), 427–462. <https://doi.org/10.1190/1.1439044>
- Keller, E. A., & Pinter, N. (1996). *Active tectonics: Earthquakes uplift and landscapes* (Vol. 333). Upper Saddle River, NJ: Prentice Hall.
- Klitgord, K. D., & Schouten, H. (1986). Plate kinematics of the central Atlantic. *Geology of North America*, 1000, 351–378. <https://doi.org/10.1130/DNAG-GNA-M.351>
- Kohfahl, C., Sprenger, C., Herrera, J. B., Meyer, H., Chacon, F. F., & Pekdeger, A. (2008). Recharge sources and hydrogeochemical evolution of groundwater in semiarid and karstic environments: A field study in the Granada Basin (Southern Spain). *Applied Geochemistry*, 23(4), 846–862. <https://doi.org/10.1016/j.apgeochem.2007.09.009>

- Koulali, A., Ouazar, D., Tahayt, A., King, R. W., Vernant, P., Reilinger, R. E., et al. (2011). New GPS constraints on active deformation along the Africa-Iberia plate boundary. *Earth and Planetary Science Letters*, 308(1–2), 211–217. <https://doi.org/10.1016/j.epsl.2011.05.048>
- Kyriakopoulos, C., Chini, M., Bignami, C., Stramondo, S., Ganas, A., Kolligri, M., & Moshou, A. (2013). Monthly migration of a tectonic seismic swarm detected by DInSAR: Southwest Peloponnese, Greece. *Geophysical Journal International*, 194(3), 1302–1309. <https://doi.org/10.1093/gji/ggt196>
- Lee, K., & Yang, W. S. (2006). Historical seismicity of Korea. *Bulletin of the Seismological Society of America*, 96(3), 846–855. <https://doi.org/10.1785/0120050050>
- Leonard, M. (2010). Earthquake fault scaling: Self-consistent relating of rupture length, width, average displacement, and moment release. *Bulletin of the Seismological Society of America*, 100(5A), 1971–1988. <https://doi.org/10.1785/0120090189>
- Llenos, A. L., McGuire, J. J., & Ogata, Y. (2009). Modeling seismic swarms triggered by aseismic transients. *Earth and Planetary Science Letters*, 281(1–2), 59–69. <https://doi.org/10.1016/j.epsl.2009.02.011>
- Lohman, R. B., & McGuire, J. J. (2007). Earthquake swarms driven by aseismic creep in the Salton Trough, California. *Journal of Geophysical Research: Solid Earth*, 112(B4), B04405. <https://doi.org/10.1029/2006JB004596>
- Luján, M. (2003). *Estructura y cinemática de la Unidad del Aljibe (Complejo de Flyschs, Béticas): Ensayo de modelización analógica*, (Doctoral dissertation). Universidad de Granada.
- Luján, M., Crespo-Blanc, A., & Balanyá, J. C. (2006). The Flysch Trough thrust imbricate (Betic Cordillera): A key element of the Gibraltar Arc orogenic wedge. *Tectonics*, 25(6), TC6001. <https://doi.org/10.1029/2005TC001910>
- Lupiani, E., & Soria, J. (1988). Mapa geológico de España a escala 1:50.000. Hoja número 1009 (Granada).
- Madarieta-Txurruka, A., Galindo-Zaldívar, J., González-Castillo, L., Peláez, J. A., Ruiz-Armenteros, A. M., Henares, J., et al. (2021). High- and low-angle normal fault activity in a collisional orogen: The Northeastern Granada Basin (Betic Cordillera). *Tectonics*, 40, e2021TC006715. <https://doi.org/10.1029/2021TC006715>
- Mancilla, F. D. L., Booth-Rea, G., Stich, D., Pérez-Peña, J. V., Morales, J., Azañón, J. M., et al. (2015). Slab rupture and delamination under the Betics and Rif constrained from receiver functions. *Tectonophysics*, 663, 225–237. <https://doi.org/10.1016/j.tecto.2015.06.028>
- Mancilla, F. D. L., Stich, D., Berrocoso, M., Martín, R., Morales, J., Fernandez-Ros, A., et al. (2013). Delamination in the Betic Range: Deep structure, seismicity, and GPS motion. *Geology*, 41(3), 307–310. <https://doi.org/10.1130/G33733.1>
- Marín-Lechado, C., Pedrera, A., Peláez, J. A., Ruiz-Constán, A., González-Ramón, A., & Henares, J. (2017). Deformation style and controlling geodynamic processes at the eastern Guadalquivir foreland basin (Southern Spain). *Tectonics*, 36(6), 1072–1089. <https://doi.org/10.1002/2017TC004556>
- Martín, R., Stich, D., Morales, J., & Mancilla, F. (2015). Moment tensor solutions for the Iberian-Maghreb region during the IberArray deployment (2009–2013). *Tectonophysics*, 663, 261–274. <https://doi.org/10.1016/j.tecto.2015.08.012>
- Martínez-Martínez, J. M., Booth-Rea, G., Azañón, J. M., & Torcal, F. (2006). Active transfer fault zone linking a segmented extensional system (Betics, southern Spain): Insight into heterogeneous extension driven by edge delamination. *Tectonophysics*, 422(1–4), 159–173. <https://doi.org/10.1016/j.tecto.2006.06.001>
- McGuire, J. J., Boettcher, M. S., & Jordan, T. H. (2005). Foreshock sequences and short-term earthquake predictability on East Pacific Rise transform faults. *Nature*, 434(7032), 457–461. <https://doi.org/10.1038/nature03377>
- McNutt, S. R. (1996). Seismic monitoring and eruption forecasting of volcanoes: A review of the state-of-the-art and case histories. In R. Scarpa, & R. I. Tilling (Eds.), *Monitoring and mitigation of volcano hazards* (pp. 99–146). Springer. [https://doi.org/10.1007/978-3-642-80087-0\\_3](https://doi.org/10.1007/978-3-642-80087-0_3)
- Meijninger, B., & Vissers, R. (2007). Thrust-related extension in the Prebetic (Southern Spain) and closure of the North Betic Strait. *Revista de la Sociedad Geológica de España*, 20(3), 153–171.
- Mogi, K. (1963). Some discussions on aftershocks, foreshocks, and earthquake swarms—The fracture of a semi-infinite body caused by an inner stress origin and its relation to the earthquake phenomena. *Bulletin of the Earthquake Research Institute, University of Tokyo*, 41(3), 615–658.
- Morales, J., Azañón, J. M., Stich, D., Roldán, F. J., Pérez-Peña, J. V., Martín, R., et al. (2015). The 2012–2013 earthquake swarm in the eastern Guadalquivir basin (South Spain): A case of heterogeneous faulting due to oroclinal bending. *Gondwana Research*, 28(4), 1566–1578. <https://doi.org/10.1016/j.gr.2014.10.017>
- Morales, J., Serrano, I., Vidal, F., & Torcal, F. (1997). The depth of the earthquake activity in the central Betics (Southern Spain). *Geophysical Research Letters*, 24(24), 3289–3292. <https://doi.org/10.1029/97GL03306>
- Morales, J., Vidal, F., De Miguel, F., Alguacil, G., Posadas, A., Ibañeiz, J., et al. (1990). Basement structure of the Granada Basin, Betic Cordilleras, Southern Spain. *Tectonophysics*, 177, 337–348. [https://doi.org/10.1016/0040-1951\(90\)90394-N](https://doi.org/10.1016/0040-1951(90)90394-N)
- Nagy, D. (1966). The gravitational attraction of a right rectangular prism. *Geophysics*, 31(2), 362–371. <https://doi.org/10.1190/1.1439779>
- NCSE-02 (2002). *Norma de construcción sismorresistente NCSE-02*. Gobierno de España, Madrid: Ministerio de Fomento, Serie Normativas, Servicio de Publicaciones.
- Nebbad, F. (2001). *Le prisme orogénique prébétique (Sud-Est de l'Espagne), évolution cinématique et coupes équilibrées*, (Doctoral dissertation). Paris XI: Univ. Orsay.
- Ocaña, E. (2009). *Análisis especial de la actividad sísmica reciente del Sur de España (spatial analysis of recent seismic activity in southern Spain)*, (Doctoral dissertation). Universidad de Granada.
- Ogata, Y. (1988). Statistical models for earthquake occurrences and residual analysis for point processes. *Journal of the American Statistical Association*, 83(401), 9–27. <https://doi.org/10.1080/01621459.1988.10478560>
- Omori, F. (1895). On the aftershocks of earthquakes. *The Journal of the College of Science, Imperial University of Tokyo*, 7, 111–200.
- Palano, M., González, P. J., & Fernández, J. (2015). The diffuse plate boundary of Nubia and Iberia in the western Mediterranean: Crustal deformation evidence for viscous coupling and fragmented lithosphere. *Earth and Planetary Science Letters*, 430, 439–447. <https://doi.org/10.1016/j.epsl.2015.08.040>
- Palomeras, I., Thurner, S., Levander, A., Liu, K., Villasenor, A., Carbonell, R., & Harnafi, M. (2014). Finite-frequency Rayleigh wave tomography of the western Mediterranean: Mapping its lithospheric structure. *Geochemistry, Geophysics, Geosystems*, 15(1), 140–160. <https://doi.org/10.1002/2013GC004861>
- Peacock, D. C. P., & Sanderson, D. J. (1991). Displacements, segment linkage, and relay ramps in normal fault zones. *Journal of Structural Geology*, 13(6), 721–733. [https://doi.org/10.1016/0191-8141\(91\)90033-F](https://doi.org/10.1016/0191-8141(91)90033-F)
- Pedrera, A., Ruiz-Constán, A., Galindo-Zaldívar, J., Chalouan, A., Sanz de Galdeano, C., Marín-Lechado, C., et al. (2011). Is there an active subduction beneath the Gibraltar orogenic arc? Constraints from Pliocene to present-day stress field. *Journal of Geodynamics*, 52(2), 83–96. <https://doi.org/10.1016/j.jog.2010.12.003>
- Platt, J., Allerton, S., Kirker, A., Mandeville, C., Mayfield, A., Platzman, E. S., & Rimi, A. (2003). The ultimate arc: Differential displacement, oroclinal bending, and vertical axis rotation in the external Betic-Rif arc. *Tectonics*, 22(3), 1017. <https://doi.org/10.1029/2001TC001321>

- Platt, J., Behr, W., Johanesen, K., & Williams, J. (2013). The Betic-Rif arc and its orogenic hinterland: A review. *Annual Review of Earth and Planetary Sciences*, 41, 313–357. <https://doi.org/10.1146/annurev-earth-050212-123951>
- Platt, J., & Vissers, R. (1989). Extensional collapse of thickened continental lithosphere: A working hypothesis for the Alboran Sea and Gibraltar Arc. *Geology*, 17(6), 540–543. [https://doi.org/10.1130/0091-7613\(1989\)017<0540:ecotcl>2.3.co;2](https://doi.org/10.1130/0091-7613(1989)017<0540:ecotcl>2.3.co;2)
- Power, J. A., Lahr, J. C., Page, R. A., Chouet, B. A., Stephens, C. D., Harlow, D. H., et al. (1994). Seismic evolution of the 1989–1990 eruption sequence of Redoubt Volcano, Alaska. *Journal of Volcanology and Geothermal Research*, 62(1–4), 69–94. [https://doi.org/10.1016/0377-0273\(94\)90029-9](https://doi.org/10.1016/0377-0273(94)90029-9)
- QAFI. (2022). Quaternary faults database of Iberia. Retrieved from <https://info.igme.es/qafi/>
- Reinhardt, L. J., Dempster, T. J., Shroder, J. F., & Persano, C. (2007). Tectonic denudation and topographic development in the Spanish Sierra Nevada. *Tectonics*, 26(3), TC3001. <https://doi.org/10.1029/2006TC001954>
- Rivas, P., Braga, J., & Sánchez-Almazo, I. (1999). Arrecifes del Tortonense inferior en la Cuenca de Granada: Cordillera Bética, España. *Trabajos de Geología*, 21, 309–321. <https://doi.org/10.17811/dg.21.1999.309-321>
- Rodríguez-Fernández, J., Azor, A., & Miguel Azañón, J. (2012). The Betic Intramontane Basins (SE Spain): Stratigraphy, subsidence, and tectonic history. In C. Busby, & A. Azor (Eds.), *Tectonics of sedimentary basins: Recent advances* (pp. 461–479). Blackwell Publishing Ltd. <https://doi.org/10.1002/9781444347166.ch23>
- Rodríguez-Fernández, J., & Sanz de Galdeano, C. (2006). Late orogenic intramontane basin development: The Granada Basin, Betics (Southern Spain). *Basin Research*, 18(1), 85–102. <https://doi.org/10.1111/j.1365-2117.2006.00284.x>
- Roland, E., & McGuire, J. J. (2009). Earthquake swarms on transform faults. *Geophysical Journal International*, 178(3), 1677–1690. <https://doi.org/10.1111/j.1365-246X.2009.04214.x>
- Rosenbaum, G., Lister, G. S., & Duboz, C. (2002). Reconstruction of the tectonic evolution of the western Mediterranean since the Oligocene. *Journal of the Virtual Explorer*, 8, 107–130. <https://doi.org/10.3809/jvirtex.2002.00053>
- Ruano, P., Galindo-Zaldívar, J., & Jabaloy, A. (2004). Recent tectonic structures in a transect of the central Betic Cordillera. *Pure and Applied Geophysics*, 161, 541–563. <https://doi.org/10.1007/s00024-003-2462-5>
- Rueda, J., & Mezcuá, J. (2005). Near-real-time seismic moment-tensor determination in Spain. *Seismological Research Letters*, 76(4), 455–465. <https://doi.org/10.1785/gssrl.76.4.455>
- Ruiz-Constán, A., Galindo-Zaldívar, J., Pedrera, A., Celerier, B., & Marín-Lechado, C. (2011). Stress distribution at the transition from subduction to continental collision (northwestern and central Betic Cordillera). *Geochemistry, Geophysics, Geosystems*, 12(12). <https://doi.org/10.1029/2011GC003824>
- Ruiz-Constán, A., Stich, D., Galindo-Zaldívar, J., & Morales, J. (2009). Is the northwestern Betic Cordillera mountain front active in the context of the convergent Eurasia-Africa plate boundary? *Terra Nova*, 21(5), 352–359. <https://doi.org/10.1111/j.1365-3121.2009.00886.x>
- Sagiya, T., Miyazaki, S., & Tada, T. (2000). Continuous GPS array and present-day crustal deformation of Japan. *Pure and Applied Geophysics*, 157(11–12), 2303–2322. [https://doi.org/10.1007/978-3-0348-7695-7\\_26](https://doi.org/10.1007/978-3-0348-7695-7_26)
- Santos-Bueno, N., Fernández-García, C., Stich, D., de Lis Mancilla, F., Martín, R., Molina-Aguilera, A., & Morales, J. (2019). Focal mechanisms for subcrustal earthquakes beneath the Gibraltar Arc. *Geophysical Research Letters*, 46(5), 2534–2543. <https://doi.org/10.1029/2018GL081587>
- Santoyo, M. A., & Luzón, F. (2008). Stress relations in three recent seismic series in the Murcia region, southeastern Spain. *Tectonophysics*, 457(1–2), 86–95. <https://doi.org/10.1016/j.tecto.2008.05.019>
- Sanz de Galdeano, C. (1990). Geologic evolution of the Betic Cordilleras in the western Mediterranean, Miocene to the present. *Tectonophysics*, 172, 107–119. [https://doi.org/10.1016/0040-1951\(90\)90062-D](https://doi.org/10.1016/0040-1951(90)90062-D)
- Sanz de Galdeano, C., & Alfaro, P. (2004). Tectonic significance of the present relief of the Betic Cordillera. *Geomorphology*, 63(3–4), 175–190. <https://doi.org/10.1016/j.geomorph.2004.04.002>
- Sanz de Galdeano, C., Andreo, B., García-Tortosa, F. J., & López-Garrido, A. C. (2001). The Triassic paleogeographic transition between the Alpujarride and Malaguide complexes. Betic-Rif Internal Zone (S Spain, N Morocco). *Paleogeography, Paleoclimatology, Paleocology*, 167(1–2), 157–173. [https://doi.org/10.1016/S0031-0182\(00\)00236-4](https://doi.org/10.1016/S0031-0182(00)00236-4)
- Sanz de Galdeano, C., García-Tortosa, F., Peláez, J. A., Alfaro, P., Azañón, J. M., Galindo-Zaldívar, J., et al. (2012). Main active faults in the Granada and Guadix-Baza Basins (Betic Cordillera). *Journal of Iberian Geology*, 38(1), 209–223. [https://doi.org/10.5209/rev\\_JIGE.2012.v38.n1.39215](https://doi.org/10.5209/rev_JIGE.2012.v38.n1.39215)
- Sanz de Galdeano, C., & Peláez, J. A. (2011). *Fallas activas en la Cordillera Bética: Una aproximación a partir de la información a partir de la información tectónica y sísmica*. Granada, Spain.
- Sanz de Galdeano, C., Peláez, J. A., & López Casado, C. (2003). Seismic potential of the main active faults in the Granada Basin (Southern Spain). *Pure and Applied Geophysics*, 160(8), 1537–1556. <https://doi.org/10.1007/s00024-003-2359-3>
- Sanz de Galdeano, C., Peláez, J. A., López Casado, C., Alfaro, P., García-Tortosa, F., Galindo-Zaldívar, J., & López-Garrido, A. C. (2010). Estudios de tectónica activa en las Cuencas de Granada y Guadix-Baza (Cordillera Bética, Sur de España). In J. M. Insua, & F. Martín González, (Eds.), *Contribución de la geología al análisis de la peligrosidad sísmica* (pp. 141–144). Sigüenza, Spain. First Iberian Meeting on Active Faults and Paleoseismology.
- Sanz de Galdeano, C., & Vera, J. A. (1991). Una propuesta de clasificación de las cuencas neógenas béticas. *Acta Geologica Hispanica*, 26(3–4), 205–227.
- Scholz, C. H. (1990). *The mechanics of earthquakes and faulting*. Cambridge University Press.
- Scholz, C. H., & Gupta, A. (2000). Fault interactions and seismic hazard. *Journal of Geodynamics*, 29(3–5), 459–467. [https://doi.org/10.1016/S0264-3707\(99\)00040-X](https://doi.org/10.1016/S0264-3707(99)00040-X)
- Seber, D., Barazangi, M., Ibrahimi, A., & Demnati, A. (1996). Geophysical evidence for lithospheric delamination beneath the Alboran Sea and rif-betic mountains. *Nature*, 379(6568), 785–790. <https://doi.org/10.1038/379785a0>
- Sempere, J. (1807). Reflexiones sobre los terremotos de Granada. Real Academia de la Historia, Ref. 9/5210, (pp. 416–453).
- Sibson, R. H. (2000). Fluid involvement in normal faulting. *Journal of Geodynamics*, 29(3–5), 469–499. [https://doi.org/10.1016/S0264-3707\(99\)00042-3](https://doi.org/10.1016/S0264-3707(99)00042-3)
- SIGEOF. (2022). *Geophysical information system*. INFOIGME. Retrieved from <http://info.igme.es/SIGEOF/>
- SIS. (2022). *Earthquake catalogue*. IGN. Retrieved from <https://www.ign.es/web/ign/portal/sis-catalogo-terremotos/>
- SMT. (2022). *Seismic moment tensor*. IGN. Retrieved from <https://www.ign.es/web/ign/portal/tensor-momento-sismico/>
- Sparacino, F., Palano, M., Peláez, J. A., & Fernández, J. (2020). Geodetic deformation vs. seismic crustal moment-rates: Insights from the Ibero-Maghrebian region. *Remote Sensing*, 12(6), 952. <https://doi.org/10.3390/rs12060952>
- Špičák, A., Förster, A., & Horsfield, B. (2005). Drilling the Eger rift in central Europe. *Scientific Drilling*, 1, 44–45. <https://doi.org/10.5194/sd-1-44-2005>



- Srivastava, S., Roest, W. R., Kovacs, L. C., Oakey, G., Levesque, S., Verhoef, J., & Macnab, R. (1990). Motion of Iberia since the late Jurassic: Results from detailed aeromagnetic measurements in the Newfoundland Basin. *Tectonophysics*, *184*(3–4), 229–260. [https://doi.org/10.1016/0040-1951\(90\)90442-B](https://doi.org/10.1016/0040-1951(90)90442-B)
- Stankova, J., Bilek, S. L., Rowe, C. A., & Aster, R. C. (2008). Characteristics of the October 2005 microearthquake swarm and reactivation of similar event seismic swarms over decadal time periods near Socorro, New Mexico. *Bulletin of the Seismological Society of America*, *98*(1), 93–105. <https://doi.org/10.1785/0120070108>
- Stein, R. S. (1999). The role of stress transfer in earthquake occurrence. *Nature*, *402*(6762), 605–609. <https://doi.org/10.1038/45144>
- Stich, D., Ammon, C. J., & Morales, J. (2003). Moment tensor solutions for small and moderate earthquakes in the Ibero-Maghreb region. *Journal of Geophysical Research: Solid Earth*, *108*(B3), 2148. <https://doi.org/10.1029/2002jb02057>
- Stich, D., Martín, R., & Morales, J. (2010). Moment tensor inversion for Iberia-Maghreb earthquakes 2005–2008. *Tectonophysics*, *483*(3–4), 390–398. <https://doi.org/10.1016/j.tecto.2009.11.006>
- Stich, D., Serpelloni, E., de Lis Mancilla, F., & Morales, J. (2006). Kinematics of the Iberia-Maghreb plate contact from seismic moment tensors and GPS observations. *Tectonophysics*, *426*(3–4), 295–317. <https://doi.org/10.1016/j.tecto.2006.08.004>
- Suarez, J. (2021). Comportamiento sísmico de los suelos. In J. Suarez (Ed.), *Deslizamientos: Análisis Geotécnico* (pp. 267–306).
- Telford, W. M., Geldart, L. P., & Sheriff, R. E. (1990). *Applied geophysics*. Cambridge University Press.
- Tendero-Salmerón, V., Galindo-Zaldívar, J., Peláez, J. A., Martínez-Martos, M., Henares, J., Marín-Lechado, C., et al. (2020). Seismicity in strike-slip foreland faults (central Betic Cordillera front): Evidence of indentation tectonics. *Tectonics*, *39*(7), 1–18. <https://doi.org/10.1029/2020TC006143>
- Thatcher, W., & Hanks, T. C. (1973). Source parameters of southern California earthquakes. *Journal of Geophysical Research*, *78*(35), 8547–8576. <https://doi.org/10.1029/jb078i035p08547>
- Turner, S., Palomeras, I., Levander, A., Carbonell, R., & Lee, C.-T. (2014). Ongoing lithospheric removal in the western Mediterranean: Evidence from Ps receiver functions and thermobarometry of Neogene basalts (PICASSO project). *Geochemistry, Geophysics, Geosystems*, *15*, 1113–1127. <https://doi.org/10.1002/2013GC005124>
- Udías, A., & Mezcua, J. (1986). *Fundamentos de Geofísica*. Universidad Complutense de Madrid.
- Vidale, J. E. (1986). Complex polarization analysis of particle motion. *Bulletin of the Seismological Society of America*, *76*(5), 1393–1405. <https://doi.org/10.1785/BSSA0760051393>
- Vidale, J. E., Boyle, K. L., & Shearer, P. M. (2006). Crustal earthquake bursts in California and Japan: Their patterns and relation to volcanoes. *Geophysical Research Letters*, *33*(20), L20313. <https://doi.org/10.1029/2006GL027723>
- Vidale, J. E., & Shearer, P. M. (2006). A survey of 71 earthquake bursts across southern California: Exploring the role of pore fluid pressure fluctuations and aseismic slip as drivers. *Journal of Geophysical Research: Solid Earth*, *111*(B5), B05312. <https://doi.org/10.1029/2005JB004034>
- Waite, G. P., & Smith, R. B. (2002). Seismic evidence for fluid migration accompanying subsidence of the Yellowstone caldera. *Journal of Geophysical Research: Solid Earth*, *107*(B9), 2177–2181. <https://doi.org/10.1029/2001JB000586>
- Waldhauser, F. (2001). HypoDD: A computer program to compute double-difference earthquake locations. <https://doi.org/10.7916/D8SN072H>
- Waldhauser, F., & Ellsworth, W. L. (2000). A double-difference earthquake location algorithm: Method and application to the Northern Hayward Fault, California. *Bulletin of the Seismological Society of America*, *90*(6), 1353–1368. <https://doi.org/10.1785/0120000006>
- Waldhauser, F., & Richards, P. G. (2004). Reference events for regional seismic phases at IMS stations in China. *Bulletin of the Seismological Society of America*, *94*(6), 2265–2279. <https://doi.org/10.1785/0120030121>
- Wells, D. L., & Coppersmith, K. J. (1994). New empirical relationships among magnitude, rupture length, rupture width, rupture area, and surface displacement. *Bulletin of the Seismological Society of America*, *84*(4), 974–1002. <https://doi.org/10.1785/BSSA0840040974>
- Wesnousky, S. G. (2008). Displacement and geometrical characteristics of earthquake surface ruptures: Issues and implications for seismic-hazard analysis and the process of earthquake rupture. *Bulletin of the Seismological Society of America*, *98*(4), 1609–1632. <https://doi.org/10.1785/0120070111>
- Willemsse, E. J., Pollard, D. D., & Aydin, A. (1996). Three-dimensional analyses of slip distributions on normal fault arrays with consequences for fault scaling. *Journal of Structural Geology*, *18*(2–3), 295–309. [https://doi.org/10.1016/S0191-8141\(96\)80051-4](https://doi.org/10.1016/S0191-8141(96)80051-4)
- Wortel, M. J. R., & Spakman, W. (1992). Structure and dynamic of subducted lithosphere in the Mediterranean. *Proceedings of the Koninklijke Nederlandse Akademie van Wetenschappen*, *95*(3), 325–347.
- Wortel, M. J. R., & Spakman, W. (2000). Subduction and slab detachment in the Mediterranean-Carpathian region. *Science*, *290*(5498), 1910–1917. <https://doi.org/10.1126/science.290.5498.1910>